Review Vol. 12, No. 7 / 1 Jul 2022 / Optical Materials Express 2724
Optical Materials EXPRESS

Nanostructured materials for circular dichroism and chirality at the nanoscale: towards unconventional characterization [Invited]

EMILIJA PETRONIJEVIC,[1,2] ALESSANDRO BELARDINI,[1,3] GRIGORE LEAHU,[1] ROBERTO LI VOTI,[1] AND CONCITA SIBILIA[1]

[1]Department S.B.A.I., Sapienza Università di Roma., Via A. Scarpa 14, I-00161, Rome, Italy
[2]emilija.petronijevic@uniroma1.it
[3]alessandro.belardini@uniroma1.it

Abstract: In this work, we review the last attempts to use nanostructured materials for the enhancement of the chiro-optical effects at the nanoscale. Starting from the numerical design, we review different geometries that exhibit circular dichroic behavior in the far field; we then focus on the new branch of near-field chirality, where numerous nanostructures have been proposed for background-free chiral sensing. The next section reports on nanofabrication methods, with a special focus on self-assembling, cost- and time-efficient techniques. Finally, we review the chiro-optical experiments. Besides conventional extinction-based techniques, we are today able to reveal chiro-optical effects via photothermal behavior and photoluminescence, going down to single nanostructure chirality with sophisticated near-field techniques. We believe that the novel designs, state-of-the-art nanofabrication and modern characterization techniques have come to a stage to provide chiro-optical sensors and light components based on nanostructures.

1. Introduction

An object is chiral if it cannot be superimposed onto its mirror image; therefore, the chiral object exists in two, left (S-) and a right (R-) versions (just like our hands), called enantiomers. Geometric definition of chirality by Lord Kelvin comes from more than a century ago, stating that there is no rotational, twisting or flipping operation which can superimpose the chiral object with its mirror image [1]. Although the two enantiomers equal in physical properties, the lack of spatial mirror symmetry makes them interact differently with the surrounding world. This difference in the interaction is present at all scales in Nature, which makes the objects in S- or R-version from galaxies in motion, down to the molecules. Most building blocks which govern the biochemistry of life are chiral: amino acids and sugars, including DNA [2]. Chirality influences biological activity and toxicity, which is extremely important in pharmacology and agrochemistry [3,4]. In a chiral drug, while one enantiomer acts as a drug, the other can remain inactive, or even lead to serious side-effects. The unfortunate example is Thalidomide, used in past to treat morning sickness in pregnant women, where the "wrong" enantiomer led to dramatic birth defects [5,6]. Other well-known commercial drugs with chirality-induced inactivity or side-effects are ibuprofene, naproxen, ketamine, methorphan, ethambutol etc [7]. Moreover, protein aggregation into chiral structures influences neurodegenerative diseases like Alzheimer's and Parkinson's, and type II diabetes [8–10]; for drug development and early diagnosis, it is indispensable to detect and image the chirality of small protein aggregates with sizes from a few nm to μm. Finally, chiral pharmaceuticals and pesticides are becoming pollutants of great concern [11,12], and chiral analysis of food and beverages sheds light on their safety, bioactivity, and quality [13]. Hence, detecting small concentrations of enantiomers by an ultra-sensitive system is essential in pharmacology, agrochemistry and medicine.

#456496 https://doi.org/10.1364/OME.456496
Journal © 2022 Received 17 Feb 2022; revised 27 Mar 2022; accepted 28 Mar 2022; published 24 Jun 2022

Optical Materials EXPRESS

Chirality of an enantiomer can be revealed through its interaction with light via chiro-optical effects: when circularly polarized (CP) light interacts with the enantiomer, its absorption rate depends on the light handedness. This is because of CP being naturally chiral, with left or right handedness (LCP or RCP, respectively). Enantiomers differently absorb LCP from RCP, and this difference is called circular dichroism (CD); a pair of enantiomers will exhibit CD spectra of the same absolute value and opposite sign [14]. The CD spectroscopy can reveal absorption differences down to 10^{-5} of the measured light intensity, and it is used to characterize the enantiomer purity in drugs, agrochemicals, food additives etc. Unfortunately, natural CD of chiral molecules is extremely low, it usually lies in the ultraviolet (UV) part of the spectrum, and the absorption vanishes at low concentrations. Conventional CD techniques are bulky, involve high enantiomer concentrations, high material waste and long integration times, and suffer from the lack of spatial resolution. Modern pharmacology would benefit from novel approaches for high enantioselectivity chiral sensing.

With the development of nanotechnology, there has been a vast interest in engineering materials at the nanoscale to enhance chiral light-matter interaction. This is because of the unique properties of nanostructures to confine light to ultra-low dimensions, where they overlap with molecules, thus providing us with a specific "zoom in" of the underlying mechanisms. The community of nanophotonics has been working in various directions where chiro-optical mechanism are used. Historically, the mimicking of chirality in nanostructures of naturally chiral shapes, such as helices and spirals, led to big CD signals in the near-infrared (near-IR) [15], visible [16] and blue range [17]. While this approach shows promise for additional degrees of freedom of far-field optical properties, such as chiral emission and lasing [17–20], one can note that the experimentally enhanced chiral sensing makes use of simpler resonant nanogeometries [21,22]. However, nanophotonic-enhanced chiral sensing with intrinsically chiral nanostructures suffers from the background CD introduced by the nanostructures' own chirality. This led to the development of a new branch of chiral nanophotonics which treats near-field chiro-optical effects in achiral nanoscale designs. Achiral resonant nanostructures have been shown to enhance molecular CD through so called superchiral near-fields. Namely, the enhanced near-field chirality is exhibited in the vicinity of the resonant nanostructure when it is excited by CP; this results in the increased difference in the absorption for RCP and LCP excitation, and leads to the enhanced CD of the chiral molecule. While abundant in numerical proposals, this approach has only recently resulted in experimental demonstrations of improved chiral sensing with enantiomers [23,24]. This shows that the nanostructure-enhanced enantioselectivity is still a hot-topic with the growing need for experimental proofs, as confirmed by very recent reviews [22,25–27].

On the other side, the industrial breakthrough of nanostructures for chiral sensing will have to eventually involve lowering of the fabrication cost of chiral sensors. One approach is to combine self-assembling approaches with some degree of asymmetry such as an oblique deposition of a plasmonic layer [28]. For example, nanosphere lithography or self-assembled nanowire (NW) growth can be combined with tilted plasmonic deposition to obtain samples with asymmetric plasmonic nanostructures, with high uniformity over large areas [29]. Additional degrees of freedom in the optical set-up can further lead to extrinsic chiral behavior even when the nanostructure is not chiral itself; this has been measured in both random self-assembled asymmetric nanostructures [30] and in periodic nanostructures forming low-cost metasurfaces [31–33]. Another very recent numerical proposal combines the in-plane anisotropy in natural hyperbolic black phosphorus, with its simple nanostructuring [34].

Development of sensitive and stable experimental approaches concerning chiro-optical phenomena keeps pace with the nanotechnology. Apart from conventional (transmission/reflection) measurements of chiral far-field properties of nanostructures [15,33,35], we can nowadays measure CD effects on photothermal response of nanostructures [30,32,36], down to single nanoparticles [37,38]. Moreover, photoluminescence measurements can reveal intrinsic [39] or

Optical Materials EXPRESS

extrinsic [40] properties of nanostructures, as well as the enhancement of near chiral fields [23]. Finally, direct insight into near field chirality is nowadays enabled by combining sophisticated scanning near-field optical microscopy (SNOM) with CD (so called CD-SNOM) [41].

In this review paper, we focus on the latest attempts to push the limits of the design, nanofabrication and experiments towardsnovel chiro-optical effects in nanostructured media. We divide the manuscript as follows: the design part first focuses on intrinsically chiral geometries and continues with the near-field effects and superchiral fields in chiral and achiral geometries. In the nanofabrication part, we start from sophisticated methods which provide nanostructures with intrinsically chiral shapes. We then focus on the lowering of the fabrication cost by means of self-assembling methods; such cost- and time-effective techniques can nowadays provide high-quality nanostructures on large areas, which exhibit both intrinsic and extrinsic chirality. Finally, we review chiro-optical measurements which lately proved giant or tunable chiral responses of nanostructures in the visible and near-IR domain. We specifically focus on non-conventional methods to reveal chiro-optical effect on photothermal response. We also comment on photoluminescence, nonlinear and near-field techniques which give circular dichroic behavior of a single nanostructure.

2. Design and simulations

Recalling the Lord Kelvin's definition of chirality, we call the system chiral if its ideal image in a plane mirror cannot be brought to coincide with itself. Natural materials manifest this property through difference in the interaction with the polarization state of the light. Namely, chiral media scatter the polarized light differently. The electromagnetic appearance of chirality is present when the medium has coupling of the electric and the magnetic field via the chirality tensor $\hat{\chi}$. Its electromagnetic response can be then described by the following constitutive relations between vectors of electric field $\vec{E}$, magnetic field $\vec{B}$, displacement field $\vec{D}$, and magnetizing field $\vec{H}$:

$$\vec{D} = \varepsilon_0 \widehat{\varepsilon_r} \vec{E} + \frac{i\hat{\chi}}{c} \vec{H}, \tag{1}$$

$$\vec{B} = \mu_0 \widehat{\mu_r} \vec{H} - \frac{i\hat{\chi}}{c} \vec{E}, \tag{2}$$

where $\widehat{\varepsilon_r}$ and $\widehat{\mu_r}$ are relative permittivity and magnetic permeability tensors, and c is the speed of light (ε_0 and μ_0 are permittivity and permeability of vacuum, respectively). For isotropic materials, all the tensor parameters become scalars, and we obtain the complex refractive indices for RCP and LCP light $\tilde{n}_{RCP}$ and $\tilde{n}_{LCP}$:

$$\tilde{n}_{RCP} = \sqrt{\varepsilon_r \mu_r} + \chi, \quad \tilde{n}_{LCP} = \sqrt{\varepsilon_r \mu_r} - \chi. \tag{3}$$

The difference in the real part of the refractive index for RCP and LCP is the circular birefringence, which leads to the well-known property of optical activity: two enantiomers will rotate the linear polarization for the same angle in opposite directions. The second property is a difference in the absorption coefficient for LCP and RCP. This effect leads to CD, and it will be mainly discussed in the following light absorbing nanostructures. Handedness dependence of the complex refractive index can be today deliberately designed in metallic, dielectric and hybrid nanostructures.

For chiral molecules in solutions, optical activity can be measured as the linear polarization tilt after the optical path which light passes through the volume of chiral medium. Otherwise, in an absorbing chiral medium, CD will be of the same value and opposite sign for the two enantiomers. However, chiral geometry in natural chiral substances occurs at pitches much lower than the pitch of the circularly polarized electromagnetic field at optical frequencies; this means that CD signals are naturally low, and such measurements require large volumes, high molecule concentrations, and large material waste. At this point, the nanotechnology offers elegant solutions for the enhancement of chiral effects by means of artificial structures at the nanoscale.

Optical Materials EXPRESS

Nanostructured materials have opened countless new possibilities by confining the electromagnetic fields to subwavelength volumes, controlling their spatial and spectral position, and enhancing the intensities in the near field. Specially engineered nanogeometries offer properties which differ from the ones of the bulk material, thus providing us with a unique "zoom in" to the processes in the near field, and their repercussions to the far field electromagnetic response. Different plasmonic, dielectric and hybrid nanostructures are nowadays studied for polarization manipulation and sensing. When it comes to chiro-optical effects, first designs involved metallic nanostructures, as they possess free electrons which couple to the electromagnetic field forming localized surface plasmons (LSP). From one side, LSPs are resonant effects where plasmonic nanostructures confine and concentrate electromagnetic fields to tiny hotspots in the near field; engineering the near field chirality is fundamental for chiral sensing platforms. From the other side, the nanostructured shapes which mimic natural chiral objects (e.g. spirals and helices) can exhibit CD when coupled with circular polarizations at normal incidence; the preferential absorption of one handedness is a consequence of intrinsic chirality. Nanostructures can nowadays be numerically designed to provide different optical response for LCP and RCP excitation, with the response being revealed in transmission, reflection, luminescence etc.

In the following, we review two fundamental branches of chiro-optical design. The first one is based on dielectric, metallic and hybrid nanostructures with chiral or asymmetric shapes which exhibit intrinsic (3D or 2D) chirality, and their CD is revealed in a far-field optical process. The second branch has lately focused on the near-field response in intrinsically achiral nanostructures. This approach makes use of the nanostructures with no intrinsic CD, but with resonant, enhanced chiro-optical effects in the near-field; these effects are sometimes defined as "superchirality", as that they can locally enhance the CD signal of the substance to be sensed.

2.1. Far-field chiro-optical effects in intrinsically chiral nanostructures

From Equations 1–2, it is clear that an artificial medium, in order to be chiral, must exhibit strong electromagnetic response; moreover, electric and magnetic resonant fields should be coupled and have parallel components, which comes naturally in 3D helices and spirals. In the case of dielectric materials, chiral crystals were historically considered for photonic band gap applications [42]. Further, the authors in [43] showed that high refractive index dielectric spirals, periodically repeated in a hexagonal lattice, show large polarization gap at normal incidence. A right handed (RH) spiral (shown in the schematic of Fig. 1(a)), exhibits predominantly left-handed eigenmodes inside the polarization gap, as demonstrated in the transmission and bandgap calculations (Fig. 1(a)). More recent numerical work [44] treated dielectric helix metasurfaces excited by light propagating perpendicularly to the helices, as in the schematics of Fig. 1(b). Their design enables functionality as a chiral mirror at normal incidence, where one circular polarization gets completely reflected without changing the polarization's handedness, the other circular polarization gets entirely transmitted, Fig. 1(b).

The pioneering experimental works in the field of 3D chiral helix-based metamaterials surely come from Karlsruhe group of professors Wegener, Linden and Freymann. They first experimentally demonstrated the idea similar to Ref. [43]. In Ref. [45], they use a low refractive index contrast polymeric helices to create 3D dielectric chiral metamaterial with evident transmission stop band at normal incidence; in Fig. 1(c), for a RH helix, there is an infrared band which almost completely blocks RCP, while strongly transmitting LCP. Numerical analysis reproduces experimental spectra with great agreement, so the authors gain insight into the electromagnetic field intensity confinement at the nanoscale. Plotting the intensity for LCP and RCP excitations at specific points of the bandgap, the matching between the incidence light and the helix handedness leads to the confinement of the light field in the helix material and a transmission gap occurs (red schematic in Fig. 1(c)).

Optical Materials EXPRESS

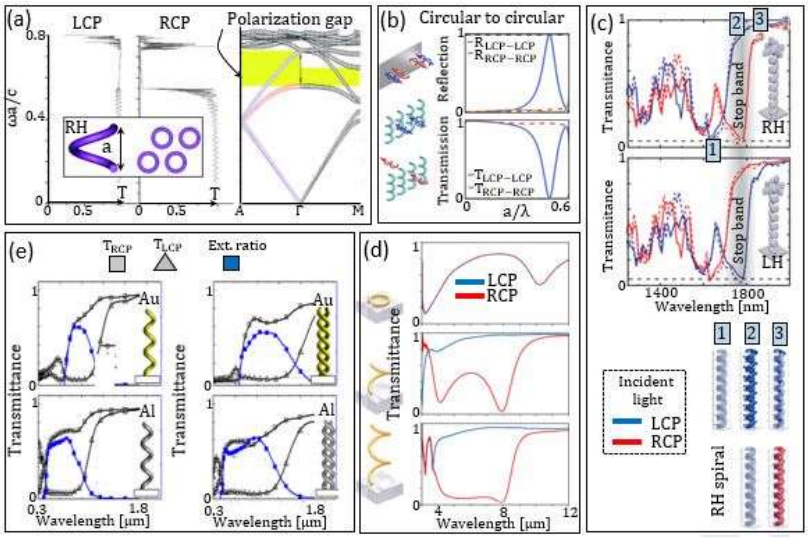

Fig. 1. 3D intrinsically chiral shapes based on helices. (a) Schematic: right-handed (RH) dielectric spiral, defined by the pitch a in the vertical direction, and arranged in the hexagonal periodic array; transmission (T) of the LCP and RCP light propagating through RH spiral confirms that the eigenmode inside the polarization gap is largely LCP. Adapted from Ref. [43]. (b) Dielectric chiral mirror: single layer helix metasurface defined by periodicity a, when excited by CP, completely reflects one polarization and preserves its handedness (e.g. LCP to LCP, blue line in the top graph), while completely transmitting another handedness (e.g. RCP to RCP, red line in the bottom graph. Adapted from Ref. [44]. (c) Top: simulated and experimental transmittance spectra of right-handed (RH) and left-handed (LH) dielectric chiral helix metamaterial, which exhibit transmission stop band in the near-IR; bottom: light intensity confinement in RH helix at specific stop band wavelengths, indicated by squares on the transmission graph. Adapted from Ref. [45]. (d) Starting from an Au achiral split-ring resonator, a one-pitch or two-pitch LH helix blocks the transmission of the same handedness, as it can be seen from red lines in transmittance graphs. Adapted from Ref. [48]. (e) Au and Al single and double helices produce broad and ultrabroad circular polarizer functionality, respectively. Results show that broadband transmittance for LCP and RCP excitation (T_{LCP} and T_{RCP}) strongly differs in the visible and near-infrared domain. Adapted from Ref. [61].

When helices are made of metal, the occurrence of chiro-optical effects becomes even more obvious; as they support coupled electric and magnetic resonances, when electric and magnetic moments become aligned, the coupling of the incident electromagnetic field depends on the match between the helix chirality and the one of the electromagnetic field. This approach was presented more than three decades ago in the featured article by Engheta and Jaggard [46], and inspired the field of chiral metamaterials in GHz region; in Ref. [47] the resonant chiral metallic helix was proposed for negative refraction. In the meantime, the nanotechnology advances allowed for dimension shrinking of the metallic helices, which allowed for chiral nanophotonic components from the infrared down to the visible range.

The first highly important experimental demonstration of the broadband circular polarizer in the infrared was based on the design from Ref. [48]: the authors start from the idea to pull one side of a split ring resonator out of the plane, thus inducing parallel electric and magnetic fields in a pitch of a helix. 3D helices are again periodically arranged in a metamaterial. The authors show that the intrinsic chirality of the helix blocks the transmission of the infrared light of the same handedness, Fig. 1(d). The same group then numerically investigated the effects of geometric

Optical Materials EXPRESS

parameters on the circular polarizer performance [49]; specifically, they give directions for the optimal design in terms of metamaterial periodicity (which should be comparable or lower from the helix pitch), metal thickness (much thinner than the helix diameter) and other parameters. Another importance of this numerical study is that it systematically shows the stability of the design when it is simulated by different simulation solvers; in particular, finite integration method in CST MICROWAVE STUDIO [50], finite difference time domain method in Lumerical [51], and finite element method in JCMsuite [52] all give consistent results in the infrared. Ever since, these solvers, with addition of COMSOL Multiphysics [53], have been used for the 3D simulation of chiro-optical response, near-field behavior and induced currents in chiral metamaterials; lately, the simulation approaches were enriched with diffractively coupled nano-antennae theory [54], inverse design method [55], deep-learning [56,57], and automatic design [58]. The invented helix-based technology further led to improvements [59] and new functionalities of helices for broadband circular polarization conversion; in [60], Wegener's group designs metamaterial based on helices of both handedness, which blocks one circular polarization, and successfully transmits and converts the other one. Another group further proposed to move chiro-optical response to the visible region, and to obtain ultrabroad circular polarizer functionality by double helix geometry [61]; in Fig. 1(e), the design of a single and double Au or Al helix metamaterial works as a broad and ultrabroad circular polarizer in the visible and near-IR ranges. Helix metamaterials are arguably the most investigated 3D chiral geometry; therefore, we direct the interested reader to comprehensive reviews on this topic [62,63].

The concept of chirality can be easily translated to 2D nanostructures, where planar chiral nanostructures lack line of symmetry in the plane. In Ref. [64], Fedotov at al. were the first ones to study intrinsic 2D nanostructure chirality in the visible and near-IR; they show that anisotropic, fish-scale Aluminum grid differently transmits LCP and RCP, with a resonance due to enantioselective plasmon, Fig. 2(a). Another intuitive chiral planar example are gammadion nanostructures, as they have a sense of twist. Ref. [65] reported on handedness-sensitive rotation of the polarization state of the incoming light, when it is diffracted from gammadion metamaterial, as in natural enantiomers. The idea was followed by numerous works which address 2D chirality in gammadions in terms of broadband optical activity [66], CD in magnetic metamaterials [67], lower loss gyrotropy [68]; in Ref. [69], the authors theoretically treat 2D chiral metamaterials as a biaxial elliptically dichroic crystals with effective dielectric tensor. Plasmonic gammadion geometry was further improved by tapering: in Ref. [70], the authors design asymmetrically tapered Au gammadion metamaterial which enhances local field distribution and extinction difference between LCP and RCP for biomolecule sensing, Fig. 2(b). Large chiro-optical effects were also obtained in simpler, L-shaped plasmonic nanostructures [71,72]. Giant visible chiral response was also demonstrated in thin, all-dielectric, lossless metamaterials: in Ref. [73], the design based on chiral Si-based metasurface led to infrared Fano resonances. In Ref. [74], Capasso's group shows that in TiO_2 gammadions on glass, magnetic and electric in-plane dipole moments possess parallel components (Fig. 2(c) left). Magnetic field has different antinodes at RCP and LCP excitation (Fig. 2(c) right), eventually leading to near-unity CD at 540 nm. Hybridizing metallic gammadion cavities with active GaN material recently led to ultraviolet room-temperature lasing with high chirality [75]; the authors show that LCP (RCP) gammadions lase into prevalently RCP (LCP) modes, due to different electromagnetic confinement in the cavity, Fig. 2(d).

Planar chirality can also be obtained in simpler nanostructures, such as plasmonic nanohole arrays. We and the co-authors recently proposed elliptical nanoholes (ENHA) which are in-plane tilted with respect to 2D array symmetry lines, Fig. 2(e). LCP and RCP light is differently absorbed at points close to surface plasmon polaritons; we optimized such arrays to a high absorption CD in the near-IR [76]. Such geometry can be further coupled with light emitting layer, for tunable luminescence with high circular polarization degree [77] Another interesting

Optical Materials EXPRESS

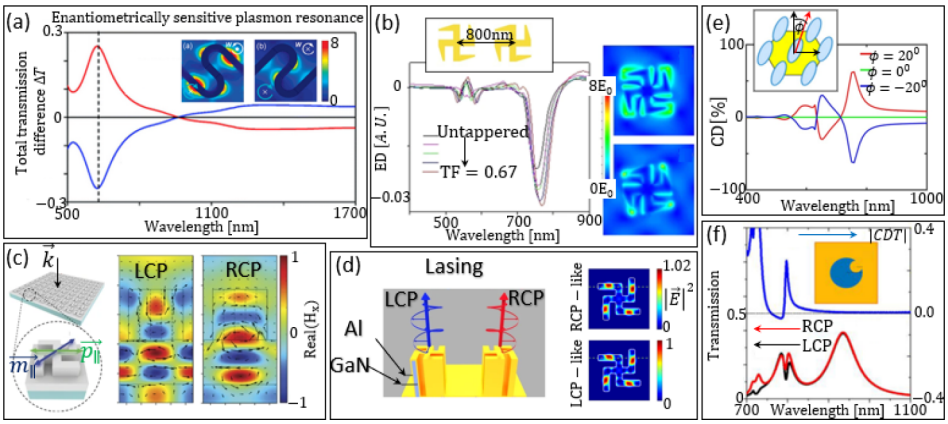

Fig. 2. 2D intrinsically chiral shapes based on helices. (a) Al fish-scale twisted 2D metamaterial differently transmits LCP and RCP, exhibiting enantioselective plasmon resonances. Total transmission difference is defined as $\Delta T = (T_{RCP} - T_{LCP})/T_{RCP}$, where $T_{LCP,RCP}$ are total transmission for LCP and RCP excitation. Red (blue) line shows ΔT in forward (backward) direction, and it is resonant around 630 nm. The inset shows different electromagnetic confinement when the metamaterial is excited with LCP from both sides. Adapted from Ref. [64]. (b) Improved design of gammadion metamaterial with tapered arms yields high extinction difference between LCP and RCP, and high near field enhancement, applied for sensing. Figure shows how the tapering fraction TF, defined as the ratio of the widths of the tapered and untapered arm, increases exctinction difference ED (given as the difference between LCP and RCP extinction) Moreover, electromagnetic field confinement is 8 times compared to the untampered version. Adapted from Ref. [70]. (c) Left: dielectric gammadions have parallel components of magnetic and electric dipole moments $\overrightarrow{m_{\parallel}}$ and $\overrightarrow{p_{\parallel}}$, thus exhibiting planar intrinsic chirality; right: different number of magnetic field (Real(H_x)) nodes for RCP and LCP excitation reveals the resonant chiral behavior in TiO_2 standing on a thin TiO_2 film on a glass substrate. Adapted from Ref. [74]. (d) Al-GaN chiral nanolasers; LCP (RCP) gammadions prevalently lase into RCP (LCP) polarization, due to the difference in the modal field, which can be appreciated by visualizing the electric field intensity $|\vec{E}|^2$ in the gammadion cross-section. Adapted from Ref. [75]. (e) Elliptical nanoholes (ENHA), tilted with respect to the array symmetry for angle φ, exhibit high absorption intrinsic chirality in the near-IR; circular dichroism is given as normalized absorption difference CD[%] = 100(A_{LCP}-A_{RCP})/(A_{LCP}+A_{RCP}), where $A_{LCP,RCP}$ are total absorption in the ENHA under LCP(RCP) excitation at normal incidence (f) Asymmetric nanohole array in silver provides large transmission difference for LCP and RCP excitation ($T_{LCP,RCP}$); here, circular dichroism in transmission is defined as CDT = (T_{LCP}-T_{RCP})/(T_{LCP}+T_{RCP}). Adapted from [78].

nanohole geometry was studied in Ref. [78]; the authors show that asymmetric nanohole array in silver can provide large transmission difference for LCP and RCP (Fig. 2(f)) and propose it for enantioseparation of chiral molecules.

Apart from intrinsically chiral nanostructure, light-matter symmetry can be broken in achiral nanostructures under oblique incidence. This so-called "extrinsic" chirality has been very popular in our community [79–85], as it allows for easier fabrication, while still providing circular dichroic behavior. However, as it includes the influence of the experimental set-up, it will be discussed further below. Finally, we believe that the future of chiral sensing relies on the use of planar rather than 3D geometries. Nanoapertures can provide electromagnetic field enhancement when covered by chiral solutions, without the mechanical and chemical instability of 3D geometries

Optical Materials EXPRESS

with the solvent. In what follows, we present different approaches to obtain and tune near-field chirality.

2.2. Near-field chirality and the quest of chiral sensing

While geometric chirality leads to far-field chiro-optical response, chiral response in the near field can be formed even around completely symmetric nanostructures. This field can be engineered and manipulated, which is of great importance for chiral sensing, with low volumes of molecules positioned in the nanostructures' vicinity. Optical chirality [86] is a physical property of any monochromatic electromagnetic wave (defined by vectors $\vec{E}$ and $\vec{B}$ at frequency ω), and it is defined as:

$$C = -0.5\varepsilon_0\omega Im\{\vec{E}^* \cdot \vec{B}\}. \tag{4}$$

In free space, CP light propagating as a plane-wave has maximum chirality, as the field vectors follow helices during propagation; C is zero for linear polarization. Near nanostructures, this factor can be enhanced by plasmonic or dielectric resonances or evanescent fields, leading to the C enhancement with respect to the CP light; this effect is sometimes called "superchirality" and it is believed to be responsible for enhanced enantioselectivity in chiral sensing.

The quest of chiral sensing started with the already mentioned gammadion nanostructures. In Ref. [87], the authors ascribe the experimental differences in gammadion CD spectrum to the adsorbed layer of chiral molecules; they numerically show that, at CD resonant wavelength, local optical chirality given by factor C can be more than 10 times higher than the one of the CP light; they recently underlined the role of structural heterogeneity for C enhancement and sensing by gammadions [88]. Kadodwala's group also showed that "shuriken" nanostructures in Au possess evanescent waves which create enhanced C; in Ref. [89], they use this effect to detect changes in the protein structure at the picogram level, coining the term "superchiral spectroscopy". This allowed for ultrasensitive (picogram) detection of the chiral molecules immersed in that field, and paved way for many novel designs of near-field factor C. In Ref. [90], Schäferling et al. investigated C enhancement in different plasmonic chiral shapes, giving the recipe for planar geometries which are more practical for sensing of the chiral substance above; Fig. 3(a) shows that for a nanospiral on a substrate, the difference in C enhancement between LCP and RCP is limited to one polarity. Chiral plasmonic nanostructures exhibiting C enhancement were lately shown to enhance chiral sensing [15], and control valley-polarized photoluminescence in MoS_2 [91]; enriching this approach with collective lattice resonances was proposed for surface-enhanced vibrational CD (VCD) [92].

Importantly, Schäferling et al. also showed that resonantly enhanced C regions can be found even around completely symmetric nanostructures, enriching simulations with a simple theoretical dipole model [93]. García-Etxarri and Dionne further provided theoretical framework for the design of near field chirality in both plasmonic and dielectric nanoantennae [94]. Nesterov et al. showed that simple, achiral plasmonic dimers (planar gap antennae) exhibit plasmon-enhanced near fields which can boost CD up to three orders of magnitude [95]. We believe that these works opened a whole new subfield of chiro-optical phenomena in nanostructures: achiral nanostructures can locally enhance optical chirality, so that chiral response of the molecules gets enhanced without the background signal of the nanostructures' CD. This idea was numerically and experimentally demonstrated in [96]: an achiral plasmonic cavity system generates and enhances a single-handed chiral near field, which means that only chiral molecules of the same handedness strongly interact with the plasmonic system, Fig. 3(b). The resulting VCD signal enhancement was around four orders of magnitude. Another geometry including surface lattice resonances in metallic nanopyramids was numerically proposed for C enhancement in high energy part of the visible spectrum, which is of interest for most pharmacologically relevant chiral molecules [97].

Optical Materials EXPRESS

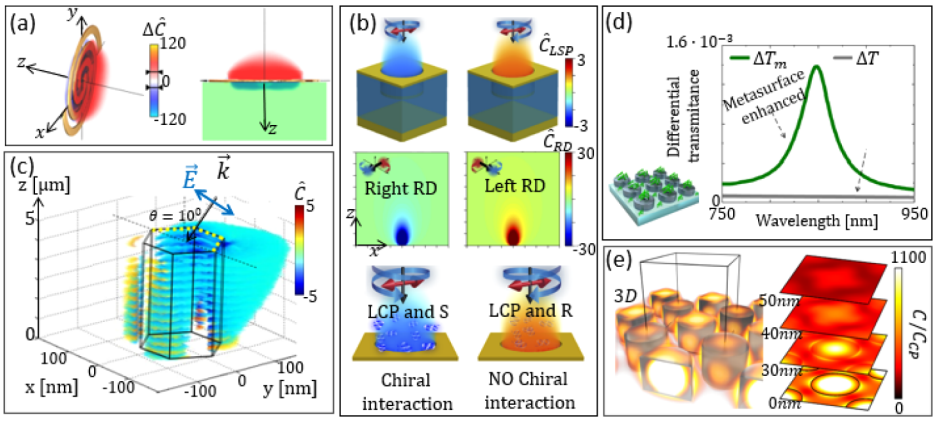

Fig. 3. Near-field chirality and factor C in plasmonic, dielectric and hybrid nanostructures. (a) Difference in LCP and RCP induced C enhancement for a plasmonic nano spiral, defined as $\Delta\hat{C}$, where $\hat{C}$ defines the optical chirality enhancement with respect to the CP light. Adapted from Ref. [90]. (b) Achiral plasmonic cavity produces the enhanced C of the same handedness, leading to stronger interaction with chiral molecules of the same handedness. Upper graph shows free space normalized localized surface plasmon (LSP) chiral near-field density distribution for LCP (blue) and RCP (red) excitations, represented in one array unit cell. Middle graph shows chiral near field cross sections for right and left rotating dipole (RD). Bottom schematic shows the idea that LCP and s-enantiomer exhibit chiral interaction, contrary to RCP and s-enantiomer. Adapted from Ref. [96]. (c) Dielectric nanowire, asymmetrically covered by Au (three out of six sidewalls), provides a same-sign C enhancement in the region around Au, even when it is excited by linear polarization at oblique incidence. (d) Si holey nanodsics covered by a chiral medium enhance its intrinsic CD in the near-IR: graph shows differential transmittance calculated as $\Delta T = 4k_0 Im\{\kappa\}w$, where k_0 is the free-space wave-number, κ is the Pasteur parameter and w is the thickness of the chiral layer deposited on the sample. It is evident that metasurface ΔT_m is resonantly enhanced with respect to the biolayer (intrinsic) differential transmittance ΔT. Adapted from Ref. [103]. (e) Diamond asymmetric achiral metasurface reaches large C enhancement in the UV. Figure shows 3D simulation of the near field optical chirality enhancements in an asymmetric disk metasurface x−y cut planes at various z heights in a single unit cell; the metasurface diameter and biperiodicity are chosen to enhance optical chirality in 260-265 nm range. Adapted from Ref. [108].

We and the co-authors investigated possibility of C enhancement with a linearly polarized light, as another background-free CD platform [98]. Fig. 3(c) shows a dielectric NW asymmetrically covered by Au; when excited by linear polarization, such platform supports leaky modes which form high C regions of the same sign around Au. If Au is functionalized with chiral molecules, this platform can be used for the sensing of both enantiomers (by inverting the incidence angle). Lately, the interest in near-field chirality moved towards lossless media [99–109] based on proper matching of dielectric and magnetic resonances via Kerker effect, and on helicity preserving all-dielectric metasurfaces in optical cavities [110,111]. In Ref. [103], the authors simulated holey Si nanodiscs covered by 20 nm of chiral molecules in water; the metasurface's near-field chirality led to 24-fold CD enhancement in the near-IR, Fig. 3(d). Moreover, designing high refractive index metasurfaces in the ultraviolet range (UV) could help to overlap CD range of pharmaceuticals with C resonances of metasurfaces. In Ref. [108], Dionne's group proposed high quality factor diamond metasurfaces; Fig. 3(e) shows great C enhancement in the volume around an asymmetric (yet achiral) metasurface in the UV. This group has since experimentally

Optical Materials EXPRESS

demonstrated that metasurfaces with optimized C factor allow for enhanced fluorescence-detected circular dichroism (FDCD) of emitting chiral molecules.

Different platforms proposed for chiral sensing [26] are based on photonic crystal with a birefringent surface defect [112], chiral surface plasmon polaritons [113,114], quasi bound states in continuum in TiO2-Au hybrid metamaterial [115] and sensing at the interface between 3D chiral helices and a hyperbolic metamaterial [116]. Even though the field is rich in numerical proposals, it was only recently that novel experimental procedures were employed to reveal the near-field optical chirality. In the near future, we can expect novel achiral designs which position C enhancement to the wavelength range of specific, relevant molecules, for industrially important applications.

3. Fabrication

3D chiral nanogeometries can be fabricated by both top-down and bottom-up methods [117], while conventional lithography techniques are usually used for 2D chiral nanostructures (and planar achiral nanostructures exhibiting near-field optical chirality). Attempts to mimic helical shapes at the micro- and nanoscale have inspired the application and development of sophisticated fabrication methods. Nowadays, the most applied ones are: direct laser writing of IR resonant nanohelix metamaterial paving the way for downscaling towards visible frequencies [45,48,59,60]; optimized glanced angle deposition on rotating substrates for regular plasmonic arrays of nanohelices [118–122]; DNA-template self-assembling for plasmonic nanohelices with CD resonances in the visible [21,123,124]; light-induced self-assembled growth of semiconductor nanoparticles into twisted shapes [125]; focused electron beam deposition and/or focused ion beam deposition for extremely versatile high quality samples with giant CD in the visible [16,62,126–130]. 3D metasurface exhibiting visible chirality was also fabricated by conventional electron beam lithography (EBL) in multiple steps, by properly twisting plasmonic nanoresonators in multiple 3D layers [131]. EBL was also combined with layer-by-layer stacking of plasmonic nanoresonators, was used to obtain chirality in 3D plasmonic oligomers [132]. Other groups made use of lower-cost focused ion beam technique, to produce Si-based metasurface corrugated in 3D in a twisted fashion [133], intrinsically chiral nanoapertures in optically thick Au film [134], 3D Archimedean spirals fabricated from stacked films [135] etc. Another highly original approach for large-area 3D printed chiral metasurfaces is based on plasmonic helical wavy ribbons on a 3D printed substrate [136]. Finally, chiro-optical response can be obtained by properly choosing and arranging different materials in planar nanotrimers [137].

Next, we focus on the approaches based on cost- and time-efficient self-assembling techniques, which could lower the cost of future chiral nanophotonic components and sensors. Firstly, chemical self-assembling of chiral nanostructures is a promising way to obtain various chiral dielectric and plasmonic shapes [138,139], of interest for both applied and basic science [140]. Next, for ordered nanostructuring into highly periodic metasurfaces, we underline the use of nanosphere lithography (NSL): a versatile, inexpensive, high-throughput technique which has been long popular among nanophotonics and especially plasmonics community. This is because it is based on commercially available nanospheres (NS) that self-assemble into a monopacked layer, with a triangular lattice constant equal to the NS diameter; starting from this layer, functionalization with plasmonic layer leads to various nanostructured shapes [141–143]. When the plasmonic deposition gets tilted, due to the shadowing effect there is a symmetry breaking in the metasurface. Belardini et al. showed that such NSL-based samples with asymmetric plasmonic shells (Fig. 4(a)), led to circular dichroism in the nonlinear optical response [144]. We later modified this approach by adding additional steps, Fig. 4(b). After the self-assembling, the NS diameter is reduced while they preserve the 2D order. The next step is the tilted plasmonic deposition, which, apart from the vertical tilt, can involve an in-plane tilt [145]. The NS can be also removed in the final step, thus leaving ENHA on the glass substrate [146]. Apart from

Optical Materials EXPRESS

being important for low-cost and large area patterning, NSL is nowadays exciting field, full of novel ideas for interesting chiral shapes. In Ref. [147], the authors perform tilted angle NSL on photoresist-coated glass substrate, thus providing chiral "nanovulcanos", Fig. 4(c). Vogel's group is a leader in the NSL-based fabrication of high quality, highly asymmetric plasmonic crescents with intriguing chiral functionalities [29,31,148,149]; in Fig. 4(d), a schematic and images of SiO_2-Au chiral crescents show that in-plane 3D tilt during NSL gives novel degrees of freedom in chiral shaping.

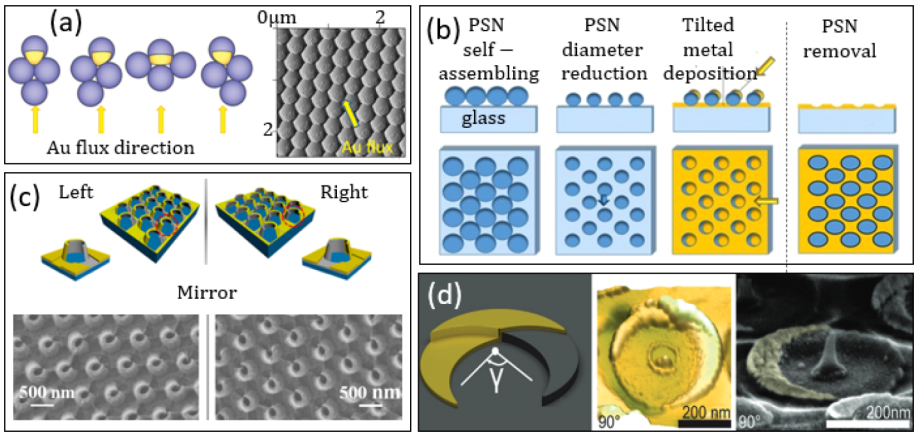

Fig. 4. Low-cost fabrication based on nanosphere lithography (NSL). (a) Oblique deposition of metallic layer leads to a metasurface with asymmetric shells [144]. Schematic shows how the choice of metallic flux direction defines the shape of the shells; on the right, a Scanning Electron Microscope (SEM) image shows one of such samples of good quality. (b) NSL with polystyrene (PSN) nanosphere shrinking, followed by a tilted angle deposition, enables fabrication of various shapes of asymmetric nanoshells. Moreover, PSN removal leaves a plasmonic array of elliptical nanoholes on the substrate (due to the shadow of the shrunken PSN). (c) Two enantiomers of chiral nanovolcanos, obtained by combining NSL on photoresist-coated glass and a tilted plasmonic deposition. Adapted from Ref. [147]. (d) Schematic (left), atomic force microscopy (middle) and false-color SEM images of SiO_2-Au chiral crescents, obtained by novel combination of in-plane tilt and shadow effects in NSL. Adapted from Ref. [148].

Other self-assembling approaches based on different starting geometries have been shown to produce CD response in the visible range. Important examples are plasmonic NWs, that can be fabricated by tilted angle deposition [81,150–152], or dielectric-based NWs asymmetrically covered by metal [30,40]. The last ones were produced by Dr. Hakkarainen and colleagues by their lithography-free self-assembling NW growth, followed by a tilted deposition of Au. This technique leads to high quality vertical NWs which have two or three sidewalls functionalized by Au. Although such NW is not intrinsically chiral, one can induce circular dichroism with the help of experimental set-up. In the following, we review experimentally observed phenomena in asymmetric samples.

4. Experiments

Chirality at the nanoscale is a growing, exciting field because the chiral light-matter interaction can have strong consequences on both far-field and near-field phenomena. Starting from basic chiro-optical characterization of nanostructures interacting with LCP/RCP, we explain typical set-ups, and move towards unconventional photothermal techniques. We finally review near-field

Optical Materials EXPRESS

characterization by means of sophisticated near-field imaging, as it directly connects to the C factor reviewed above.

4.1. Chiral characterization by means of transmission/reflection

A typical chiro-optical set-up is made of a light source, polarizing components, rotation stage, and photodetectors, Fig. 5(a). An input beam is CP polarized by a set of linear polarizer (LP) and a quarter wave plate (QWP); LCP or RCP light interacts with the nanostructure and one measures differences in transmission or reflection in the output. Another pair of QWP and LP can be on the pathway of the output (transmitted or reflected signal) to resolve it in polarization. Conventional transmission CD spectroscopy (by commercial CD spectrometer Applied Photophysics Chirascan) was done under normal incidence for different nanostructure-chiral molecule systems to explore possibility of improved chiral sensing. Specifically, remarkable effects of nanostructure-enhanced CD were proved for systems of achiral nanostructures coupled with chiral molecules. In Ref. [153], the authors report on CD enhancement of chiral riboflavin molecules via their near-field interaction with achiral Au nanostructures. In Ref. [154], achiral plasmonic metamaterial made of Au nanorods provides CD enhancement of chiral mercury sulfide nanocrystals; the same chiral medium was recently coupled with achiral dielectric nanospheres [155], leading to an important experimental proof of near-field chirality enhancement (as presented above in Section 2.2).

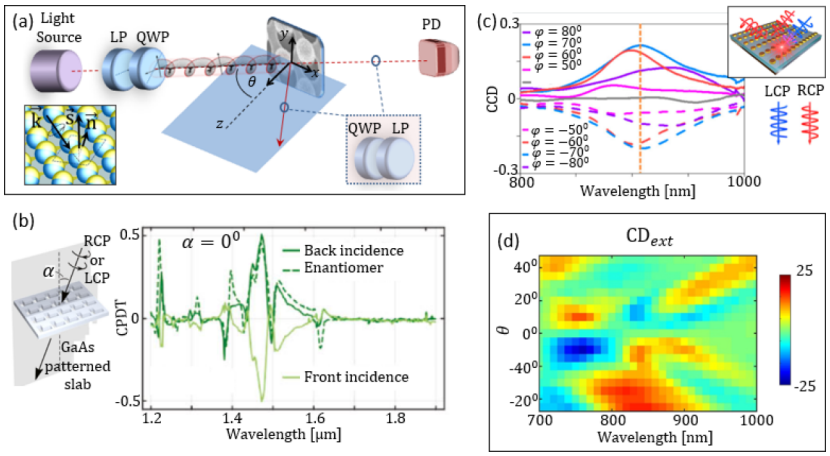

Fig. 5. (a) An input of a typical chiro-optical set-up is a light beam, polarized with set of linear polarizer (LP) and quarter wave plate (QWP). Circularly polarized light (CP) interacts with nanostructure, possibly on a rotation stage, and differences in transmission or reflection are monitored in the output. The output signal can also be CP-resolved. (b) Differential transmission of left and right CP (LCP and RCP) light at normal incidence reveals intrinsic chirality of L-shaped nanoholes in dielectric (CPDT = T_{LCP}-T_{RCP}). Adapted from Ref. [156]. (c) Extrinsic chirality in achiral metasurface based on Au nanodiscs leads to circular conversion dichroism (CCD), which is easily tunable by oblique incidence and in-plane tilt angle ϕ; CCD is defined as a difference between $R_{--}$and R_{++}, where R_{--} (R_{++}) is a ratio of LCP (RCP) excitation which gets reflected into LCP (RCP). Adapted from [160]. (d) Broadband characterization of extrinsic chirality in low-cost NSL-based metasurface, with CD_{ext} given as $100(Ext_{LCP}-Ext_{RCP})/(Ext_{LCP}+Ext_{RCP})$; $Ext_{LCP(RCP)}$ are extinction signals for LCP(RCP) excitations [33].

If the nanostructure is not intrinsically chiral, we can still have CD response by "inducing" it in the set-up. The extrinsic chirality is obtained by breaking the mirror symmetry between the light wave vector $\vec{k}$, the surface normal $\vec{s}$ and the average asymmetry vector $\vec{n}$, which must form a non-planar triad of vectors. In practice, this means that we might need additional degrees of

Optical Materials EXPRESS

freedom in the set-up such as oblique incidence and in-plane rotation of the sample (to properly orientate its "asymmetry" given by $\vec{n}$, inset of Fig. 5(a)).

Zanotto et al. recently performed important study on CP-dependent transmission and revealed intrinsic and extrinsic interplay of chirality in dielectric metasurfaces [156,157]. They found that L-shaped holes in a dielectric slab exhibit band structure and superchirality; in Fig. 5(b), differential transmission (CPDT = T_{LCP}-T_{RCP}) is shown at normal incidence, revealing the expected intrinsic chirality. Measurements of differential LCP/RCP transmission were already implemented in chiral sensing measurements [15,158].

On the other hand, when the nanostructure is not transmitting, CD is characterized by measuring differential absorption by means of reflection (A = 1-R). In Ref. [159], the authors measured back-reflection from intrinsically chiral plasmonic nanostructures, and calculated CD as CD = A_{LCP}-A_{RCP}. We recently measured extrinsic chirality in GaAs-based NWs asymmetrically covered by Au; we used LCP and RCP excitation at oblique incidence, and monitored the total intensity of specular reflection [35]. The reflected signal can further be resolved by a circular analyzer for the characterization of helicity preserving; Mao et al. recently showed that completely symmetric metasurface based on Au disks can work as a chiral mirror if manipulated with extrinsic chirality [160]. At fixed oblique incidence ($\theta = 45^0$), they tilt the plane of incidence with respect symmetry lines for angle φ, and they measure circular conversion dichroism (CCD) defined as CCD = $R_{--}R_{++}$, where R_{--} (R_{++}) is a ratio of LCP (RCP) excitation which gets reflected into LCP (RCP), Fig. 5(c).

We recently measured extinction in low-cost metasurfaces produced by NSL approach [33]; polystyrene NS are asymmetrically covered by Au and have an ENHA on the glass substrate due to the shadowing effect. The widely tunable near-IR laser is CP polarized and directed under oblique incidence towards the metasurface. Extinction maps for LCP and RCP polarization revealed rich, lattice-governed resonant behavior resembling the one of chiral surface lattice resonances. Here we define extinction CD_{ext} as $100(Ext_{LCP}-Ext_{RCP})/(Ext_{LCP}+Ext_{RCP})$, where $Ext_{LCP(RCP)}$ are extinction signals for LCP(RCP) excitations. Extinction CD reaches 24% in the near-IR (Fig. 5(d)), and can be further optimized by modelling. We believe that this resonant behavior shows great promise for tunable chiral emission (through coupling with a nearby fluorescent layer [33]). However, these samples are not suitable for chiral sensing because of the instability of polystyrene with solvents used in chiral solutions [161]. To this end, we are currently working on NSL-based samples without PS, as such ENHA are easier to couple with the chiral medium to be sensed.

4.2. Photo-thermal techniques

A natural definition of circular dichroic behavior in materials comes from the differential absorption between LCP and RCP. In scattering nanostructures, this means that the proper measurement of CD would involve precise and contemporary transmission and reflection measurements also of the scattered light, which becomes more complicated when extrinsic chirality is involved. Instead, photo-thermal effects can directly reveal the light absorption via its influence on the generated heat [36]. Here we review photo-acoustic spectroscopy (PAS), photothermal deflection technique (PDT) and CD thermal lens as alternative, non-destructive, scattering-free means to reveal CD in nanostructures.

PAS is based on a non-radiative process of heat generation when a sample absorbs light. If the sample is in a photo-acoustic cell, and the intensity of light gets modulated in time, the heating cycles correspond to periodic change of pressure. These pressure changes produce an acoustic signal which is detected by a microphone. As the light does not arrive to the microphone directly, the influence of the scattering is largely reduced. Moreover, this technique has been long used for its simplicity, stability, low-cost, and no need for complicated post-processing [162–166]. Here we show the use of PAS for extrinsic chirality characterization, Fig. 6(a). The

Optical Materials EXPRESS

laser light is modulated in time by a chopper, LCP or RCP polarized and sent onto a sample in a PAS cell. Under oblique incidence and proper orientation of the non-planar triad of vectors, an asymmetric sample differently absorbs LCP and RCP, thus giving a real value of CD as a differential absorption. We define CD [%] as $100*(A_{LCP}-A_{RCP})/(A_{LCP}+A_{RCP})$, where A_{LCP} (A_{RCP}) is PAS signal for LCP (RCP) excitation. We show typical CD for three samples of GaAs-based NW asymmetrically covered by Au at 532 nm [30,167] and for low-cost metasurfaces fabricated by NSL at 633 nm [145]. Broadband characterization of resonant CD behavior of these materials can be in future performed by combining the PAS set-up with the widely tunable laser (Fig. 5(d)).

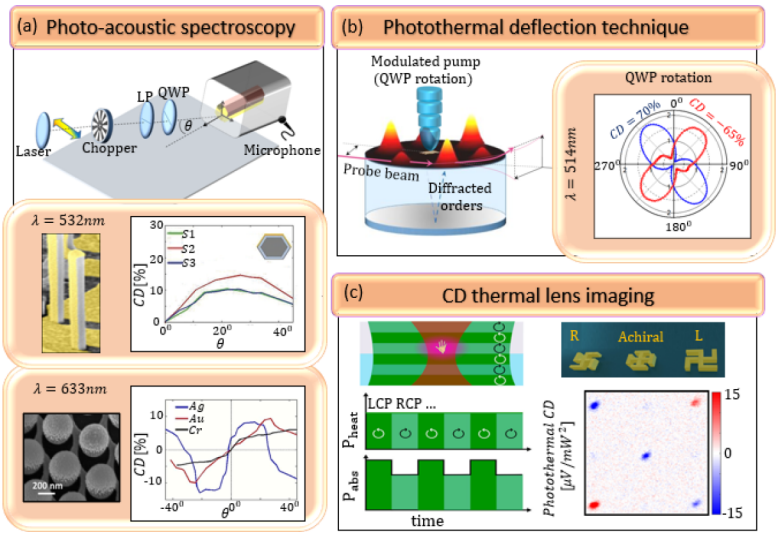

Fig. 6. (a) Photo-acoustic spectroscopy can be used for scattering-free detection of absorption CD in nanomaterials. CD [%] is defined as $100*(A_{LCP}-A_{RCP})/(A_{LCP}+A_{RCP})$, where A_{LCP} (A_{RCP}) is PAS signal for LCP (RCP) excitation. Two examples for extrinsic CD measurements are shown for GaAs-based NWs asymmetrically covered by Au at 532 nm [30], and low-cost asymmetric NSL-based metasurfaces at 633 nm [145]. (b) Photo-deflection technique can reveal chiro-optical properties of diffractive metasurfaces: pump beam induces handedness-dependent diffracted beams, which get reflected from the mirror below back to the surface, where they are absorbed; probe beam then detects local temperature change due to this absorption. Polar plot shows QWP dependence of two orders at 514 nm [32]. (c) Thermal lens imaging, combined with modulation of polarization between LCP and RCP, is able to sense CD of individual chiral nanoparticles. Adapted from Ref. [37].

While PAS measures total absorption in the sample, PDT can be used to access local information on the generated heat. It is based on a mirage effect: a pump beam gets absorbed on the substrate, and a probe beam gets deflected due to this absorption-induced temperature gradient. In very recent experiments [32,168], we applied PDT to study chirality in diffractive metasurfaces. We positioned a diffractive metasurface on a mirror; the visible light pump beam, modulated in time, gets diffracted from a metasurface, the diffracted orders reflect back from the mirror, and get absorbed on the surface. In this way, hexagonal lattice produces ordinary pattern of heat sources on the substrate, which then deflect a probe beam, Fig. 6(b). The intensity of PDT deflection is tightly related to handedness-dependent diffraction in a specific order; as shown in the polar plot, two neighboring orders at 514 nm show high CD of the opposite sign; note that CD is defined as before, but for the local, handedness-dependent absorption of the single order exiting on the

Optical Materials EXPRESS

substrate. We hope that our approach could lead to novel applications of PDT as a low-cost alternative to diffraction spectroscopy [169,170].

Finally, a highly sensitive photothermal microscopy can implemented with CD for the sensing of single chiral plasmonic nanostructures. Following the idea in the older work by Kitamori's group [171], Spaeth et al. have recently invented a new way to look at CD of single particles [37], schematically shown in Fig. 6(c). They use a wide heating beam (in green) and a tightly focused probe beam (in red); the heating beam is modulated in polarization between LCP and RCP by an electro optical modulator. The absorbed power generates thermal lens around the object, and the probe beam measures the strength of thermal lens. Individual left- and right-handed gammadions exhibit opposite values of photothermal CD, Fig. 6(c), while achiral nanostructures exhibit none. The importance of this idea lies in the possibility to measure local temperature dependence on the incoming polarization state, again, without scattering.

In conclusion, photothermal techniques open new perspectives in characterization and understanding of chiral absorption at the nanoscale and solve problems of conventional techniques which involve scattering, damage, and difficult post-processing. The community would largely benefit from the possibility of broadband characterization of photothermal effects by these methods.

4.3. *Chiral photoluminescence, nonlinear effects and near-field techniques*

An important branch of chiral optics focuses on generating circularly polarized states from chiral structures which emit light. Perfect examples are intrinsically chiral geometries where an active light emitting material such as GaN lies inside a chiral plasmonic geometry such as gammadion [75] or spiral [17]. Engineering the circular polarization degree of the emitted light and making it tunable has been recently recognized in groups directed towards quantum technologies. For example, Bozhevolnyi and co-workers used chiral hybrid nanoridge-based metasurface to generate single photons in the visible [18]; they also implemented handedness dependence of quantum emitters in plasmonic nanocircuitry [19]. Looking at simpler geometries, Hakkarainen et al. investigated the output polarization of the GaAs emission from Au-GaAs asymmetric NWs. Since the asymmetric Au layer breaks the symmetry in the available modes, a circular polarization degree at oblique emission arises from the extrinsic chirality [40]. Photoluminescence can also be a tool to sense CD-induced effects in nanostructures functionalized with emitters or with emitting chiral molecules. In Ref. [39], the authors look at the consequences of photothermal chirality in plasmonic helicoids by luminescence radio thermometry. Another approach, highly important for chiral sensing, is the use of achiral, all-dielectric, nanostructured platforms in FDCD technique [23]; Dionne's group revealed the connection of the enhanced absorption rate due to optimized C factor, and the fluorescence intensity of emitting chiral molecules. Their work thus proved the importance of the C-enhancement engineering for ultrasensitive chiral molecule sensing.

Nonlinear optics community has also been active in investigation of chiro-optical effects. This is expected as higher harmonics are usually more sensitive to the lack of symmetry than their linear counterparts, and do not require matching between electric and magnetic resonances [172]. Moreover, plasmonic chiro-optical enhancement occurs at the interfaces and surfaces of chiral nanostructures, thus being a great reason for sensing with nonlinear techniques. Valev and co-workers demonstrated orientation-dependent second harmonic generation (SHG) in G-shaped nanostructures [173, 174] and their combination in plasmonic ratchet wheels [175]. They also investigated Au-based nanohelices in terms of giant SHG anisotropies [176]. We showed that SHG in GaAs-Au hybrid asymmetric NWs depends on the incidence handedness and its spectral match with the NW resonant modes [177]. Recently, Valev and co-workers have made remarkable progress in chiro-optical measurements of higher order nonlinearities of chiral forms in liquids. Specifically, they were first to experimentally demonstrate the effect of optical activity in hyper-Rayleigh scattering (HRS), the theory of which was proposed more than 40 years ago

Optical Materials EXPRESS

in Ref. [178]; they investigate Ag nanohelices in water and demonstrate large enhancement of HRS optical activity in second [179] and third [180] harmonic. Finally, in a very recent work, they investigate semiconductor nanohelices and observe optical activity of third harmonic Mie scattering in ultrasmall volumes, thus opening new paths towards ultrasensitive chiral sensing [181].

All the mentioned unconventional techniques give us information of chiro-optical coupling from different points of view, usually revealing the consequences of nanoscale chirality on optical or photothermal signals. Moreover, near-field CD phenomena can nowadays be visualized by adapting scanning near-field optical microscope (SNOM) for chiral measurements. Okamoto's group is leader in CD-SNOM imaging of single nanostructures in the visible domain; their approach involves collection-mode aperture-type SNOM combined with photo-elastic modulator, which produces CD contrast images. In Ref. [41], they sense S- and O-shaped single nanostructures at three visible wavelengths, showing high local ellipticity in the center of chiral nanostructures. More importantly, in [182,183] they demonstrate local near field chirality in completely symmetric nanostructures, thus encouraging the research presented in Section 2.2. Another group performed CD-SNOM imaging on intrinsically chiral nanostructures in IR [184]. CD-SNOM is an elegant combination of developed CD and SNOM techniques which could be in future directly related to the C enhancement engineering; we therefore hope that it will soon become conventional imaging characterization of nanostructures.

5. Conclusion

In this work, we reviewed the development of chiro-optical effects in nanostructures by separating design from fabrication and experiments. We believe that all three counterparts: design, nanofabrication, and experiments, have nowadays reached the level at which chiro-optical properties can be used in real life applications.

As for the design, different 3D and planar chiral geometries have been proposed for chiro-optical phenomena in the far-field. Numerical investigation of such platforms shows is essential for numerous applications in chiro-optical control; these span from chip-scale, "flat optics" alternative to bulky optical components, all the way to nanosources which emit with deliberately chosen degree of circular polarization (of importance for optical, and, in future, quantum information). Nowadays, however, we note a separate branch of nanophotonic design which focuses on the near-field chirality for sensing applications. Although starting from near fields in chiral plasmonic nanostructures, this branch is now fast evolving with all-dielectric, achiral solutions which provide background-free CD enhancement.

On the fabrication side, sophisticated nanostructuring techniques have been used to obtain high quality samples exhibiting chiro-optical effects. However, the industrial breakthrough of nanostructures for chiral sensing and chiro-optical control will eventually require simpler and cheaper nanotechnology. Therefore, after presenting the most popular conventional fabrication, we underlined the use of self-assembling techniques which are cost- and time-efficient, while still providing good quality samples.

We further commented on different conventional experimental approaches, which demonstrate high intrinsic and extrinsic chiral properties of nanostructures. However, when it comes to coupling of nanostructures with chiral substances, we believe that there is a lot of space for improvement in the field; our community needs systematic, precise and repeatable studies of improved chiral sensing capabilities. Finally, we focused on novel, scattering-free, photothermal techniques which are able to directly show circular dichroic behavior of the nanostructured samples. We can conclude that the current vast multidisciplinary scientific experitise regarding design ideas, nanotechnological development and experimental procedures are ready to be brought together towards chiro-optical manipulation at the nanoscale, finally leading to industrially relevant applications.

Optical Materials EXPRESS

Disclosures. The authors declare no conflicts of interest.

Data availability. Data availability. No data were generated or analyzed in the presented research.

References

1. Lord Kelvin, in *Baltimore Lectures on Molecular Dynamics and the Wave Theory of Light* (Clay and Sons. (1904), p. 449.
2. M. Wang, P. Zhou, J. Wang, Y. Zhao, H. Ma, J. R. Lu, and H. Xu, "Left or right: how does amino acid chirality affect the handedness of nanostructures self-assembled from short amphiphilic peptides?" J. Am. Chem. Soc. **139**(11), 4185–4194 (2017).
3. A. J. Hutt and S. C. Tan, "Drug chirality and its clinical significance," Drugs **52**(Supplement 5), 1–12 (1996).
4. L. A. Nguyen, H. He, and C. Pham-Huy, "Chiral drugs: an overview," Adv. Nat. Sci.: Nanosci. Nanotechnol. **2**(2), 85–100 (2006).
5. M. E. Franks, G. R. Macpherson, and W. D. Figg, "Thalidomide," Lancet **363**(9423), 1802–1811 (2004).
6. E. Tokunaga, T. Yamamoto, E. Ito, and N. Shibata, "Understanding the thalidomide chirality in biological processes by the self-disproportionation of enantiomers," Sci. Rep. **8**(1), 17131 (2018).
7. J. T. Collins, C. Kuppe, D. C. Hooper, C. Sibilia, M. Centini, and V. K. Valev, "Chirality and chiroptical effects in metal nanostructures: fundamentals and current trends," Adv. Opt. Mater. **5**(16), 1700182 (2017).
8. N. Gao, Z. Du, Y. Guan, K. Dong, J. Ren, and X. Qu, "Chirality-selected chemical modulation of amyloid aggregation," J. Am. Chem. Soc. **141**(17), 6915–6921 (2019).
9. C. M. Dobson, "Protein folding and misfolding," Nature **426**(6968), 884–890 (2003).
10. D. J. Cordato, L. E. Mather, and G. K. Herkes, "Stereochemistry in clinical medicine: a neurological perspective," J. Clin. Neurosci. **10**(6), 649–654 (2003).
11. Y. Zhou, S. Wu, H. Zhou, H. Huang, J. Zhao, Y. Deng, H. Wang, Y. Yang, J. Yang, and L. Luo, "Chiral pharmaceuticals: Environment sources, potential human health impacts, remediation technologies and future perspective," Environ. Int. **121**(1), 523–537 (2018).
12. P. Jeschke, "Current status of chirality in agrochemicals," Pest Manage. Sci. **74**(11), 2389–2404 (2018).
13. G. Alvarez-Rivera, Monica Bueno, D. Ballesteros-Vivas, and A. Cifuentes, "Chiral analysis in food science," TrAC, Trends Anal. Chem. **123**, 115761 (2020).
14. A. Rodger and B. Nordén, *Circular Dichroism and Linear Dichroism* (Oxford Univ. Press, 1997).
15. Y. Zhao, A.N. Askarpour, L. Sun, J. Shi, X. Li, and A. Alù, "Chirality detection of enantiomers using twisted optical metamaterials," Nat. Commun. **8**(1), 14180 (2017).
16. M. Esposito, V. Tasco, M. Cuscunà, F. Todisco, A. Benedetti, I. Tarantini, M. De Giorgi, D. Sanvitto, and A. Passaseo, "Nanoscale 3D chiral plasmonic helices with circular dichroism at visible frequencies," ACS Photonics **2**(1), 105–114 (2015).
17. W.-C. Liao, S.-W. Liao, K.-J. Chen, Y.-H. Hsiao, S.-W. Chang, H.-C. Kuo, and M.-H. Shih, "Optimized spiral metal-gallium-nitride nanowire cavity for ultra-high circular dichroism ultraviolet lasing at room temperature," Sci. Rep. **6**(1), 26578 (2016).
18. Y. Kan, S. K. H. Andersen, F. Ding, S. Kumar, C. Zhao, and S. I. Bozhevolnyi, "Metasurface-enabled generation of circularly polarized single photons," Adv. Mater. **32**(16), 1907832 (2020).
19. Y. Kan, S. Kumar, F. Ding, C. Zhao, and S. I. Bozhevolnyi, "Spin–orbit controlled excitation of quantum emitters in hybrid plasmonic nanocircuits," Adv. Opt. Mater. **8**(21), 2000854 (2020).
20. S. Schanne, P. Suffit, E. Filloux, A. Lhuillier, and Degiron, "Spontaneous emission of vector vortex beams," Phys. Rev. Appl. **14**(6), 064077 (2020).
21. X.-T. Kong, L. V. Besteiro, Z. Wang, and A. O. Govorov, "Plasmonic chirality and circular dichroism in bioassembled and nonbiological systems: theoretical background and recent progress," Adv. Mater. **32**(41), 1801790 (2020).
22. L. A. Warning, A. R. Miandashti, L. A. McCarthy, Q. Zhang, C. F. Landes, and Stephan Link, "Nanophotonic approaches for chirality sensing," ACS Nano **15**(10), 15538–15566 (2021).
23. M. L. Solomon, J. M. Abendroth, L. V. Poulikakos, J. Hu, and J. A. Dionne, "Fluorescence-detected circular dichroism of a chiral molecular monolayer with dielectric metasurfaces," J. Am. Chem. Soc. **142**(43), 18304–18309 (2020).
24. T. Xiao, Z. Cheng, Z. Luo, A. Isozaki, K. Hiramatsu, T. Itoh, M. Nomura, S. Iwamoto, and K. Goda, "All-dielectric chiral-field-enhanced Raman optical activity," Nat. Commun. **12**(1), 3062 (2021).
25. H. Zhang, S. Li, A. Qu, C. Hao, M. Sun, L. Xu, C. Xu, and H. Kuang, "Engineering of chiral nanomaterials for biomimetic catalysis," Chem. Sci. **11**(48), 12937–12954 (2020).
26. A. Kakkanattu, N. Eerqing, S. Ghamari, and F. Vollmer, "Review of optical sensing and manipulation of chiral molecules and nanostructures with the focus on plasmonic enhancements," Opt. Express **29**(8), 12543–12579 (2021).
27. J. Kim, A. S. Rana, Y. Kim, I. Kim, T. Badloe, M. Zubair, and M. Q. MehmoodJ. Rho, "Chiroptical metasurfaces: principles, classification, and applications," Sensors **21**(13), 4381 (2021).
28. B. Ai and Y. Zhao, "Glancing angle deposition meets colloidal lithography: a new evolution in the design of nanostructures," Nanophotonics **8**(1), 1–26 (2018).
29. E.S.A. Goerlitzer, A. S. Puri, J. J. Moses, L. V. Poulikakos, and N. Vogel, "The beginner's guide to chiral plasmonics: mostly harmless theory and the design of large-area substrates," Adv. Opt. Mater. **9**(16), 2100378 (2021).

Optical Materials EXPRESS

30. G. Leahu, E. Petronijevic, A. Belardini, M. Centini, C. Sibilia, T. Hakkarainen, E. Koivusalo, M. Rizzo Piton, S. Suomalainen, and M. Guina, "Evidence of optical circular dichroism in GaAs-based nanowires partially covered with gold," Adv. Opt. Mater. **5**(16), 1601063 (2017).
31. E.S.A. Goerlitzer, R. Mohammadi, S. Nechayev, K. Volk, M. Rey, P. Banzer, M. Karg, and N. Vogel, "Chiral surface lattice resonances," Adv. Mater. **32**(22), 2001330 (2020).
32. G. Leahu, E. Petronijevic, R. Li Voti, A. Belardini, T. Cesca, G. Mattei, and C. Sibilia, "Diffracted beams from metasurfaces: high chiral detectivity by photothermal deflection technique," Adv. Opt. Mater. **9**(21), 2100670 (2021).
33. E. Petronijevic, A. Belardini, T. Cesca, C. Scian, G. Mattei, and C. Sibilia, "Rich near-infrared chiral behavior in diffractive metasurfaces," Phys. Rev. Appl. **16**(1), 014003 (2021).
34. N. Matthaiakakis, S. Droulias, and G. Kakarantzas, "Dynamic control of light chirality with nanostructured monolayer black phosphorus for broadband terahertz applications," Adv. Opt. Mater. **10**(5), 2102273 (2022).
35. E. Petronijevic, A. Belardini, G. Leahu, T. Hakkarainen, M. Rizzo Piton, E. Koivusalo, and C. Sibilia, "Broadband optical spin dependent reflection in self-assembled GaAs-based nanowires asymmetrically hybridized with Au," Sci. Rep. **11**(1), 4316 (2021).
36. X.-T. Kong, L.K. Khorashad, Z. Wang, and A.O. Govorov, "Photothermal circular dichroism induced by plasmon resonances in chiral metamaterial absorbers and bolometers," Nano Lett. **18**(3), 2001–2008 (2018).
37. P. Spaeth, S. Adhikari, L. Le, T. Jollans, S. Pud, W. Albrecht, T. Bauer, M. Caldarola, L. Kuipers, and M. Orrit, "Circular dichroism measurement of single metal nanoparticles using photothermal imaging," Nano Lett. **19**(12), 8934–8940 (2019).
38. P. Spaeth, S. Adhikari, M. Dieter Baaske, S. Pud, J. Ton, and M. Orrit, "Photothermal circular dichroism of single nanoparticles rejecting linear dichroism by dual modulation," ACS Nano **15**(10), 16277–16285 (2021).
39. A.R. Miandashti, L.K. Khorashad, M.E. Kordesch, A.O. Govorov, and H.H. Richardson, "Experimental and theoretical observation of photothermal chirality in gold nanoparticle helicoids," ACS Nano **14**(4), 4188–4195 (2020).
40. T. Hakkarainen, E. Petronijevic, M. Rizzo Piton, and C. Sibilia, "Demonstration of extrinsic chirality of photoluminescence with semiconductor-metal hybrid nanowires," Sci. Rep. **9**(1), 5040 (2019).
41. T. Narushima and H. Okamoto, "Circular dichroism nano-imaging of two-dimensional chiral metal nanostructures," Phys. Chem. Chem. Phys. **15**(33), 13805 (2013).
42. O. Toader and S. John, "Proposed square spiral microfabrication architecture for large three-dimensional photonic band gap crystals," Science **292**(5519), 1133–1135 (2001).
43. J. Lee and C.T. Chan, "Polarization gaps in spiral photonic crystals," Opt. Express **13**(20), 8083–8088 (2005).
44. I. Karakasoglu, M. Xiao, and S. Fan, "Polarization control with dielectric helix metasurfaces and arrays," Opt. Express **26**(17), 21664–21674 (2018).
45. M. Thiel, M. Decker, M. Deubel, M. Wegener, S. Linden, and G. von Freymann, "Polarization stop bands in chiral polymeric three-dimensional photonic crystals," Adv. Mater. **19**(2), 207–210 (2007).
46. N. Engheta and D. L. Jaggard, "Electromagnetic chirality and its applications," IEEE Antennas Propag. Soc. Newsl. **30**(5), 6–12 (1988).
47. J.B. Pendry, "A chiral route to negative refraction," Science **306**(5700), 1353–1355 (2004).
48. J.K. Gansel, M. Thiel, M. S. Rill, M. Decker, K. Bade, V. Saile, G. von Freymann, S. Linden, and M. Wegener, "Gold Helix Photonic Metamaterial as Broadband Circular Polarizer," Science **325**(5947), 1513–1515 (2009).
49. J.K. Gansel, M. Wegener, S. Burger, and Stefan Linden, "Gold helix photonic metamaterials: A numerical parameter study," Opt. Express **18**(2), 1059–1069 (2010).
50. https://www.3ds.com/products-services/simulia/products/cst-studio-suite/solvers/
51. https://www.lumerical.com/
52. https://www.jcmwave.com
53. https://www.comsol.com/
54. R. Wang, C. Forestiere, and L. Dal Negro, "Radiative properties of diffractively-coupled optical nano-antennas with helical geometry," Opt. Express **23**(20), 25496–25508 (2015).
55. C. Liu, Y. Bai, J. Zhou, Q. Zhao, Y. Yang, H. Chen, and L. Qiao, "High-performance bifunctional polarization switch chiral metamaterials by inverse design method," npj Comput. Mater. **5**(1), 93 (2019).
56. E. Ashalley, K. Acheampong, L. V. Besteiro, P. Yu, A. Neogi, A. O. Govorov, and Z. M. Wang, "Multitask deep-learning-based design of chiral plasmonic metamaterials," Photonics Res. **8**(7), 1213–1225 (2020).
57. X. Liao, L. Gui, Z. Yu, T. Zhang, and K. Xu, "Deep learning for the design of 3D chiral plasmonic metasurfaces," Opt. Mater. Express **12**(2), 758–771 (2022).
58. L. Beretta, S. Bonfanti, J. Fiocchi, F. Font-Clos, R. Guerra, A. Tuissi, and S. Zapperi, "Automatic design of chiral mechanical metamaterials," APL Mater. **9**(10), 101112 (2021).
59. J. Kaschke, M. Blome, S. Burger, and M. Wegener, "Tapered N -helical metamaterials with three-fold rotational symmetry as improved circular polarizers," Opt. Express **22**(17), 19936–19946 (2014).
60. J. Kaschke, L. Blume, L. Wu, M. Thiel, K. Bade, Z. Yang, and M. Wegener, "A helical metamaterial for broadband circular polarization conversion," Adv. Opt. Mater. **3**(10), 1411–1417 (2015).
61. Z. Y. Yang, M. Zhao, P. X. Lu, and Y. F. Lu, "Ultrabroadband optical circular polarizers consisting of double-helical nanowire structures," Opt. Lett. **35**(15), 2588–2590 (2010).

Optical Materials EXPRESS

62. A. Passaseo, M. Esposito, M. Cuscunà, and V. Tasco, "Materials and 3D designs of helix nanostructures for chirality at optical frequencies," Adv. Opt. Mater. **5**(16), 1601079 (2017).
63. M. Qiu, L. Zhang, Z. Tang, W. Jin, C.-W. Qiu, and D.Y. Le, "3D metaphotonic nanostructures with intrinsic chirality," Adv. Funct. Mater. **28**(45), 1803147 (2018).
64. V.A. Fedotov, A.S. Schwanecke, N.I. Zheludev, V.V. Khardikov, and S.L. Prosvirnin, "Asymmetric transmission of light and enantiomerically sensitive plasmon resonance in planar chiral nanostructures," Nano Lett. **7**(7), 1996–1999 (2007).
65. A. Papakostas, A. Potts, D. M. Bagnall, S.L. Prosvirnin, H.J. Coles, and N.I. Zheludev, "Optical manifestations of planar chirality," Phys. Rev. Lett. **90**(10), 107404 (2003).
66. M. Kuwata-Gonokami, N. Saito, Y. Ino, M. Kauranen, K. Jefimovs, T. Vallius, J. Turunen, and Y. Svirko, "Giant optical activity in quasi-two-dimensional planar nanostructures," Phys. Rev. Lett. **95**(22), 227401 (2005).
67. M. Decker, M. W. Klein, M. Wegener, and S. Linden, "Circular dichroism of planar chiral magnetic metamaterials," Opt. Lett. **32**(7), 856–858 (2007).
68. E. Plum, V.A. Fedotov, A.S. Schwanecke, N. I. Zheludev, and Y. Chen, "Giant optical gyrotropy due to electromagnetic coupling," Appl. Phys. Lett. **90**(22), 223113 (2007).
69. S.V. Zhukovsky, A.V. Novitsky, and V.M. Galynsky, "Elliptical dichroism: operating principle of planar chiral metamaterials," Opt. Lett. **34**(13), 1988–1990 (2009).
70. E.H. Khoo, E.S.P. Leong, S. J. Wu, W.K. Phua, Y.L. Hor, and Y. J. Liu, "Effects of asymmetric nanostructures on the extinction difference properties of actin biomolecules and filaments," Sci. Rep. **6**(1), 19658 (2016).
71. A. B. Khanikaev, N. Arju, Z. Fan, D. Purtseladze, F. Lu, J. Lee, P. Sarriugarte, M. Schnell, R. Hillenbrand, M. A. Belkin, and G. Shvets, "Experimental demonstration of the microscopic origin of circular dichroism in two-dimensional metamaterials," Nat. Commun. **7**(1), 12045 (2016).
72. W. Ye, X. Yuan, C. Guo, J. Zhang, B. Yang, and S. Zhang, "Large chiroptical effects in planar chiral metamaterials," Phys. Rev. Appl. **7**(5), 054003 (2017).
73. C. Wu, N. Arju, G. Kelp, J.A. Fan, J. Dominguez, E. Gonzales, E. Tutuc, I. Brener, and G. Shvets, "Spectrally selective chiral silicon metasurfaces based on infrared Fano resonances," Nat. Commun. **5**(1), 3892 (2014).
74. A.Y. Zhu, W.T. Chen, A. Zaidi, Y.-W. Huang, M. Khorasaninejad, V. Sanjeev, C.-W. Qiu, and F. Capasso, "Giant intrinsic chiro-optical activity in planar dielectric nanostructures," Light: Sci. Appl. **7**(2), 17158 (2018).
75. C.-L. Yu, Y.-H. Hsiao, C.-Y. Chang, P.-J. Cheng, H.-T. Lin, M.-S. Lai, H.-C. Kuo, S.-W. Chang, and M.-H. Shih, "High circular polarized nanolaser with chiral gammadion metal cavity," Sci. Rep. **10**(1), 7880 (2020).
76. E. Petronijevic, H. Ali, N. Zaric, A. Belardini, G. Leahu, T. Cesca, G. Mattei, L. C. Andreani, and C. Sibilia, "Chiral efects in low-cost plasmonic arrays of elliptic nanoholes," Opt. Quantum Electron. **52**(3), 176 (2020).
77. E. Petronijevic, R. Ghahri, and C. Sibilia, "Plasmonic elliptical nanohole arrays for chiral absorption and emission in the near-infrared and visible range," Appl. Sci. **11**(13), 6012 (2021).
78. H.A. Arredondo Champi, R.H. Bustamante, and W.J. Salcedo, "Optical enantioseparation of chiral molecules using asymmetric plasmonic nanoapertures," Opt. Mater. Express **9**(4), 1763–1775 (2019).
79. E. Plum, V.A. Fedotov, and N.I. Zheludev, "Extrinsic electromagnetic chirality in metamaterials," J. Opt. A: Pure Appl. Opt. **11**(7), 074009 (2009).
80. E. Plum, X.-X. Liu, V.A. Fedotov, Y. Chen, D.P. Tsai, and N.I. Zheludev, "Metamaterials: optical activity without chirality," Phys. Rev. Lett. **102**(11), 113902 (2009).
81. A. Belardini, M.C. Larciprete, M. Centini, E. Fazio, C. Sibilia, D. Chiappe, C. Martella, A. Toma, M. Giordano, and F. Buatier de Mongeot, "Circular dichroism in the optical second-harmonic emission of curved gold metal nanowires," Phys. Rev. Lett. **107**(25), 257401 (2011).
82. T. Cao and M.J. Cryan, "Enhancement of circular dichroism by a planar non-chiral magnetic metamaterial," J. Opt. **14**(8), 085101 (2012).
83. I. De Leon, M.J. Horton, S.A. Schulz, J. Upham, P. Banzer, and R.W. Boyd, "Strong, spectrally-tunable chirality in diffractive metasurfaces," Sci. Rep. **5**(1), 13034 (2015).
84. E. Plum, "Extrinsic chirality: Tunable optically active reflectors and perfect absorbers," Appl. Phys. Lett. **108**(24), 241905 (2016).
85. E. Petronijevic, S.A. Dereshgi, M.C. Larciprete, M. Centini, C. Sibilia, and K. Aydin, "Extrinsic chirality and circular dichroism at visible frequencies enabled by birefringent α-MoO_3 nanoscale-thick films: implications for chiro-optical control," ACS Appl. Nano Mater. accepted (2022).
86. Y. Tang and A. E. Cohen, "Optical chirality and its interaction with matter," Phys. Rev. Lett. **104**(16), 163901 (2010).
87. E. Hendry, T. Carpy, J. Johnston, M. Popland, R.V. Mikhaylovskiy, A.J. Lapthorn, S.M. Kelly, L.D. Barron, N. Gadegaard, and M. Kadodwala, "Ultrasensitive detection and characterization of biomolecules using superchiral fields," Nat. Nanotechnol. **5**(11), 783–787 (2010).
88. C. Gilroy, D.J.P. Koyroytsaltis-McQuire, N. Gadegaard, A.S. Karimullah, and M. Kadodwala, "Superchiral hot-spots in ''real'' chiral plasmonic structures," Mater. Adv. **3**(1), 346–354 (2022).
89. R. Tullius, A.S. Karimullah, M. Rodier, B. Fitzpatrick, N. Gadegaard, L.D. Barron, V.M. Rotello, G. Cooke, A. Lapthorn, and M. Kadodwala, ""Superchiral" spectroscopy: detection of protein higher order hierarchical structure with chiral plasmonic nanostructures," J. Am. Chem. Soc. **137**(26), 8380–8383 (2015).

Optical Materials EXPRESS

90. Schäferling, Dregely, Hentschel, and Giessen, "Tailoring enhanced optical chirality: design principles for chiral plasmonic nanostructures," Phys. Rev. X **2**, 031010 (2012).
91. Z. Li, C. Liu, X. Rong, Y. Luo, H. Cheng, L. Zheng, F. Lin, B. Shen, Y. Gong, S. Zhang, and Z. Fang, "Tailoring MoS_2 valley-polarized photoluminescence with super chiral near-field," Adv. Mater. **30**(34), 1801908 (2018).
92. F. Mattioli, G. Mazzeo, G. Longhi, S. Abbate, G. Pellegrini, E. Mogni, M. Celebrano, M. Finazzi, L. Duò, C.G. Zanchi, M. Tommasini, M. Pea, S. Cibella, R. Polito, F. Sciortino, L. Baldassarre, A. Nucara, M. Ortolani, and P. Biagioni, "Plasmonic superchiral lattice resonances in the mid-infrared," ACS Photonics **7**(10), 2676–2681 (2020).
93. X. Schäferling, H. Yin, and Giessen, "Formation of chiral fields in a symmetric environment," Opt. Express **20**(24), 26326–26336 (2012).
94. A. García-Etxarri and J.A. Dionne, "Surface-enhanced circular dichroism spectroscopy mediated by nonchiral nanoantennas," Phys. Rev. B **87**(23), 235409 (2013).
95. M. L. Nesterov, X. Yin, M. Schäferling, H. Giessen, and T. Weiss, "The role of plasmon-generated near fields for enhanced circular dichroism spectroscopy," ACS Photonics **3**(4), 578–583 (2016).
96. A. Vázquez-Guardado and D. Chanda, "Superchiral Light Generation on Degenerate Achiral Surfaces," Phys. Rev. Lett. **120**(13), 137601 (2018).
97. E. Petronijevic, E. M. Sandoval, M. Ramezani, C. L. Ordóñez-Romero, C. Noguez, F. A. Bovino, C. Sibilia, and G. Pirruccio, "Extended chiro-optical near-field response of achiral plasmonic lattices," J. Phys. Chem. C **123**(38), 23620–23627 (2019).
98. E. Petronijevic, M. Centini, A. Belardini, G. Leahu, T. Hakkarainen, and C. Sibilia, "Chiral near-field manipulation in Au-GaAs hybrid hexagonal nanowires," Opt. Express **25**(13), 14148 (2017).
99. H. Chi-Sing Ho, A. García-Etxarri, Y. Zhao, and J. Dionne, "Enhancing enantioselective absorption using dielectric nanospheres," ACS Photonics **4**(2), 197–203 (2017).
100. Xin Zhao, M.H. Alizadeh, and B. M. Reinhard, "Generating optical birefringence and chirality in silicon nanowire dimers," ACS Photonics **4**(9), 2265–2273 (2017).
101. M.L. Solomon, J. Hu, M. Lawrence, A. García-Etxarri, and J. Dionne, "Enantiospecific optical enhancement of chiral sensing and separation with dielectric metasurfaces," ACS Photonics **6**(1), 43–49 (2019).
102. E. Mohammadi, K.I. Tsakmakidis, A.N. Askarpour, P. Dehkhoda, A. Tavakoli, and H. Altug, "Nanophotonic platforms for enhanced chiral sensing," ACS Photonics **5**(7), 2669–2675 (2018).
103. E. Mohammadi, A. Tavakoli, P. Dehkhoda, Y. Jahani, K. L. Tsakmakidis, A. Tittl, and H. Altug, "Accessible superchiral near-fields driven by tailored electric and magnetic resonances in all-dielectric nanostructures," ACS Photonics **6**(8), 1939–1946 (2019).
104. X. Zhao and B.M. Reinhard, "sSwitchable chiroptical hot-spots in silicon nanodisk dimers," ACS Photonics **6**(8), 1981–1989 (2019).
105. L.V. Poulikakos, J.A. Dionne, and A. García-Etxarri, "Optical helicity and optical chirality in free space and in the presence of matter," Symmetry **11**(9), 1113 (2019).
106. E. Petronijevic and C. Sibilia, "Enhanced near-field chirality in periodic arrays of Si nanowires for chiral sensing," Molecules **24**(5), 853 (2019).
107. T. V. Raziman, R. H. Godiksen, M. A. Müller, and A. G. Curto, "conditions for enhancing chiral nanophotonics near achiral nanoparticles," ACS Photonics **6**(10), 2583–2589 (2019).
108. J. Hu, M. Lawrence, and J. Dionne, "high quality factor dielectric metasurfaces for ultraviolet circular dichroism spectroscopy," ACS Photonics **7**(1), 36–42 (2020).
109. J. Lasa-Alonso, D. R. Abujetas, Á. Nodar, J. Dionne, J. J. Saenź, G. Molina-Terriza, J. Aizpurua, and A. García-Etxarri, "Surface-enhanced circular dichroism spectroscopy on periodic dual nanostructures," ACS Photonics **7**(11), 2978–2986 (2020).
110. D. Beutel, P. Scott, M. Wegener, C. Rockstuhl, and I. Fernandez-Corbaton, "Enhancing the optical rotation of chiral molecules using helicity preserving all-dielectric metasurfaces," Appl. Phys. Lett. **118**(22), 221108 (2021).
111. P. Scott, X. Garcia-Santiago, D. Beutel, C. Rockstuhl, M. Wegener, and I. Fernandez-Corbaton, "On enhanced sensing of chiral molecules in optical cavities," Appl. Phys. Rev. **7**(4), 041413 (2020).
112. G. Pellegrini, M. Finazzi, M. Celebrano, L. Duò, and P. Biagioni, "Chiral surface waves for enhanced circular dichroism," Phys. Rev. B **95**(24), 241402 (2017).
113. A.A. Saleh and J. A. Dionne, "Toward efficient optical trapping of sub-10-nm particles with coaxial plasmonic apertures," Nano Lett. **12**(11), 5581–5586 (2012).
114. M. Alizadeh and B.R.M. Reinhard, "Transverse chiral optical forces by chiral surface plasmon polaritons," ACS Photonics **2**(12), 1780–1788 (2015).
115. Yang Chen, Chen Zhao, Yongzhe Zhang, and Cheng-wei Qiu, "Integrated molar chiral sensing based on high-q metasurface," Nano Lett. **20**, 8696–8703 (2020).
116. G. Palermo, G.E. Lio, M. Esposito, L. Ricciardi, M. Manoccio, V. Tasco, A. Passaseo, A. De Luca, and Giuseppe Strangi, "Biomolecular sensing at the interface between chiral metasurfaces and hyperbolic metamaterials," ACS Appl. Mater. Interfaces **12**(27), 30181–30188 (2020).
117. M. Hentschel, M. Schäferling, X. Duan, H. Gieseen, and N. Liu, "Chiral plasmonics," Sci. Adv. **3**(5), 1602735 (2017).
118. J. M. Caridad, D. McCloskey, J. F. Donegan, and V. Krstić, "Controllable growth of metallic nano-helices at room temperature conditions," Appl. Phys. Lett. **105**(23), 233114 (2014).

Optical Materials EXPRESS

119. S. Eslami, J.G. Gibbs, Y. Rechkemmer, J. van Slageren, M. Alarcón-Correa, T. Lee, A. G. Mark, G. L. J. A. Rikken, and P. Fischer, "Chiral nanomagnets," ACS Photonics **1**(11), 1231–1236 (2014).
120. J.M. Caridad, S. Winters, D. McCloskey, G.S. Duesberg, J.F. Donegan, and V. Krstić, "Hot-volumes as uniform and reproducible SERS-detection enhancers in weakly-coupled metallic nanohelices," Sci. Rep. **7**(1), 45548 (2017).
121. M. Matuschek, D.P. Singh, H. Jeong, M. Nesterov, T. Weiss, P. Fischer, F. Neubrech, and N. Liu, "Chiral Plasmonic Hydrogen Sensors," Small **14**(7), 1702990 (2018).
122. J. M. Caridad, C. Tserkezis, J. E. Santos, P. Plochocka, M. Venkatesan, J. M. D. Coey, N.A. Mortensen, G. L. J. A. Rikken, and V. Krstić, "Detection of the Faraday chiral anisotropy," Phys. Rev. Lett. **126**(17), 177401 (2021).
123. A. Kuzyk, R. Schreiber, Z. Fan, G. Pardatscher, E. Roller, A. Högele, F.C. Simmel, A.O. Govorov, and T. Liedl, "DNA-based self-assembly of chiral plasmonic nanostructures with tailored optical response," Nature **483**(7389), 311–314 (2012).
124. X. Lan, T. Liu, Z. Wang, A.O. Govorov, H. Yan, and Y. Liu, "DNA-guided plasmonic helix with switchable chirality," J. Am. Chem. Soc. **140**(37), 11763–11770 (2018).
125. S. Srivastava, A. Santos, K. Critchley, K. Kim, P. Podsiadlo, K. Sun, J. Lee, C. Xu, G.D. Lilly, S.C. Glotzer, and N.A. Kotov, "Light-controlled self-assembly of semiconductor nanoparticles into twisted ribbons," Science **327**(5971), 1355–1359 (2010).
126. M. Esposito, V. Tasco, F. Todisco, M. Cuscunà, A. Benedetti, D. Sanvitto, and A. Passaseo, "Triple-helical nanowires by tomographic rotatory growth for chiral photonics," Nat. Commun. **6**(1), 6484 (2015).
127. V. Tasco, M. Esposito, F. Todisco, A. Benedetti, M. Cuscunà, D. Sanvitto, and A. Passaseo, "Three-dimensional nanohelices for chiral photonics," Appl. Phys. A **122**(4), 280 (2016).
128. M. Esposito, V. Tasco, F. Todisco, M. Cuscunà, A. Benedetti, M. Scuderi, G. Nicotra, and A. Passaseo, "Programmable extreme chirality in the visible by helix-shaped metamaterial platform," Nano Lett. **16**(9), 5823–5828 (2016).
129. M. Manoccio, M. Esposito, E. Primiceri, A. Leo, V. Tasco, M. Cuscunà, D. Zuev, Y. Sun, G. Maruccio, A. Romano, A. Quattrini, G. Gigli, and A. Passaseo, "Femtomolar biodetection by a compact core−shell 3D chiral metamaterial," Nano Lett. **21**(14), 6179–6187 (2021).
130. M. Esposito, M. Manoccio, A. Leo, M. Cuscunà, Y. Sun, E. Ageev, D. Zuev, A. Benedetti, I. Tarantini, A. Passaseo, and V. Tasco, "3D Chiral MetaCrystals," Adv. Funct. Mater. **32**(12), 2109258 (2021).
131. Y. Zhao, M.A. Belkin, and A. Alù, "Twisted optical metamaterials for planarized ultrathin broadband circular polarizers," Nat. Commun. **3**(1), 870 (2012).
132. M. Hentschel, M. Schäferling, T. Weiss, N. Liu, and H. Giessen, "Three-dimensional chiral plasmonic oligomers," Nano Lett. **12**(5), 2542–2547 (2012).
133. M. V. Gorkunov, O.Y. Rogov, A.V. Kondratov, V.V. Artemov, R.V. Gainutdinov, and A.A. Ezhov, "Chiral visible light metasurface patterned in monocrystalline silicon by focused ion beam," Sci. Rep. **8**(1), 11623 (2018).
134. Y. Chen, X. Yang, and J. Gao, "Spin-controlled wavefront shaping with plasmonic chiral geometric metasurfaces," Light: Sci. Appl. **7**(1), 84 (2018).
135. M.L. Tseng, Z. Lin, H.Y. Kuo, T. Huang, Y. Huang, T.L. Chung, C.H. Chu, J. Huang, and D.P. Tsai, "Stress-induced 3D chiral fractal metasurface for enhanced and stabilized broadband near-field optical chirality," Adv. Opt. Mater. **7**(15), 1900617 (2019).
136. S.V. Golod, V.A. Seyfi, A.F. Buldygin, A.E. Gayduk, and V.Y. Prinz, "Large-area 3D-printed chiral metasurface composed of metal helices," Adv. Opt. Mater. **6**(19), 1800424 (2018).
137. P. Banzer, P. Woźniak, U. Mick, I. De Leon, and R.W. Boyd, "Chiral optical response of planar and symmetric nanotrimers enabled by heteromaterial selection," Nat. Commun. **7**(1), 13117 (2016).
138. A. Ben-Moshe, S. Grayer Wolf, M. Bar Sadan, L. Houben, Z. Fan, A.O. Govorov, and Gil Markovich, "Enantioselective control of lattice and shape chirality in inorganic nanostructures using chiral biomolecules," Nat. Commun. **5**(1), 4302 (2014).
139. H.-E. Lee, H. Ahn, J. Mun, Y.Y. Lee, M. Kim, N.H. Cho, K. Chang, W.S. Kim, J. Rho, and K.T. Nam, "Amino-acid- and peptide-directed synthesis of chiral plasmonic gold nanoparticles," Nature **556**(7701), 360–365 (2018).
140. A. Ben-Moshe, A. da Silva, Alexander Müller, A. Abu-Odeh, P. Harrison, J. Waelder, F. Niroui, C. Ophus, A.M. Minor, M. Asta, W. Theis, P. Ercius, and A.P. Alivisatos, "The chain of chirality transfer in tellurium nanocrystals," Science **372**(6543), 729–733 (2021).
141. V. Robbiano, M. Giordano, C. Martella, F.D. Stasio, D. Chiappe, F. Buatier de Mongeot, and D. Comoretto, "Hybrid plasmonic–photonic nanostructures: gold nanocrescents over opals," Adv. Opt. Mater. **1**(5), 389–396 (2013).
142. T. Cesca, N. Michieli, B. Kalinic, A. Sanchez-Espinoza, M. Rattin, V. Russo, V. Mattarello, C. Scian, P. Mazzoldi, and G. Mattei, "Nonlinear absorption tuning by composition control in bimetallic plasmonic nanoprism arrays," Nanoscale **7**(29), 12411–12418 (2015).
143. V. Russo, N. Michieli, T. Cesca, C. Scian, D. Silvestri, M. Morpurgo, and G. Mattei, "Gold–silver alloy semi-nanoshell arrays for label-free plasmonic biosensors," Nanoscale **9**(28), 10117–10125 (2017).
144. A. Belardini, A. Benedetti, M. Centini, G. Leahu, F. Mura, S. Sennato, C. Sibilia, V. Robbiano, M.C. Giordano, C. Martella, D. Comoretto, and F. Buatier de Mongeot, "Second harmonic generation circular dichroism from self-ordered hybrid plasmonic–photonic nanosurfaces," Adv. Opt. Mater. **2**(3), 208–213 (2014).
145. E. Petronijevic, G. Leahu, R. Li Voti, A. Belardini, C. Scian, N. Michieli, T. Cesca, G. Mattei, and C. Sibilia, "Photo-acoustic detection of chirality in metal-polystyrene metasurfaces," Appl. Phys. Lett. **114**(5), 053101 (2019).

Optical Materials EXPRESS

146. E. Petronijevic, A. Belardini, G. Leahu, T. Cesca, C. Scian, G. Mattei, and C. Sibilia, "Circular dichroism in low-cost plasmonics: 2D arrays of nanoholes in silver," Appl. Sci. **10**(4), 1316 (2020).
147. Y. Guan, Z. Wang, B. Ai, C. Chen, W. Zhang, Y. Wang, and G. Zhang, "Chiral plasmonic metamaterials with tunable chirality," ACS Appl. Mater. Interfaces **12**(44), 50192–50202 (2020).
148. E.S.A. Goerlitzer, R. Mohammadi, S. Nechayev, P. Banzer, and N. Vogel, "Large-area 3D plasmonic crescents with tunable chirality," Adv. Opt. Mater. **7**(15), 1801770 (2019).
149. E.S.A. Goerlitzer, L.E. Speichermann, T.A. Mirza, R. Mohammadi, and N. Vogel, "Addressing the plasmonic hotspot region by site-specific functionalization of nanostructures," Nanoscale Adv. **2**(1), 394–400 (2020).
150. A. Belardini, M.C. Larciprete, M. Centini, E. Fazio, C. Sibilia, M. Bertolotti, A. Toma, D. Chiappe, and F. Buatier De Mongeot, "Tailored second harmonic generation from self-organized metal nanowires arrays," Opt. Express **17**(5), 3603–3609 (2009).
151. A. Belardini, M. Centini, G. Leahu, D.C Hooper, R. Li Voti, E. Fazio, J.W Haus, A. Sarangan, V.K. Valev, and C. Sibilia, "Chiral light intrinsically couples to extrinsic/pseudo-chiral metasurfaces made of tilted gold nanowires," Sci. Rep. **6**(1), 31796 (2016).
152. A. Belardini, M. Centini, G. Leahu, E. Fazio, C. Sibilia, J.W. Haus, and A. Sarangan, "Second harmonic generation on self-assembled tilted gold nanowires," Faraday Discuss. **178**, 357–362 (2015).
153. B.M. Maoz, Y. Chaikin, A.B. Tesler, O. Bar Elli, Z. Fan, A.O. Govorov, and G. Markovich, "Amplification of chiroptical activity of chiral biomolecules by surface plasmons," Nano Lett. **13**(3), 1203–1209 (2013).
154. D. Vestler, I. Shishkin, E.A. Gurvitz, M.E. Nasir, A. Ben-Moshe, A.P. Slobozhanyuk, A.V. Krasavin, T. Levi-Belenkova, A.S. Shalin, P. Ginzburg, G. Markovich, and A. V. Zayats, "Circular dichroism enhancement in plasmonic nanorod metamaterials," Opt. Express **26**(14), 17841–17848 (2018).
155. D. Vestler, A. Ben-Moshe, and Gil Markovich, "Enhancement of circular dichroism of a chiral material by dielectric nanospheres," J. Phys. Chem. C **123**(8), 5017 (2019).
156. S. Zanotto, G. Mazzamuto, F. Riboli, G. Biasiol, G.C. La Rocca, A. Tredicucci, and A. Pitanti, "Photonic bands, superchirality, and inverse design of a chiral minimal metasurface," Nanophotonics **8**(12), 2291–2301 (2019).
157. S. Zanotto, A. Tredicucci, D. Navarro-Urrios, M. Cecchini, G. Biasiol, D. Mencarelli, L. Pierantoni, and A. Pitanti, "Optomechanics of chiral dielectric metasurfaces," Adv. Opt. Mater. **8**(4), 1901507 (2020).
158. Y. Mazhdi and S.M. Hamidi, "Detection of scorpion venom by optical circular dichroism method," Sci. Rep. **11**(1), 15854 (2021).
159. L. Ouyang, W. Wang, D. Rosenmann, D.A. Czaplewski, J. Gao, and X. Yang, "Near-infrared chiral plasmonic metasurface absorbers," Opt. Express **26**(24), 31484 (2018).
160. L. Mao, K. Liu, S. Zhang, and T. Cao, "Extrinsically 2D-chiral metamirror in near-infrared region," ACS Photonics **7**(2), 375–383 (2020).
161. A. Belardini, E. Petronijevic, R. Ghahri, D. Rocco, F. Pandolfi, C. Sibilia, and L Mattiello, "Fluorescence spectroscopy of enantiomeric amide compounds enforced by chiral light," Appl. Sci. **11**(23), 11375 (2021).
162. R. Li Voti, G. Leahu, M.C. Larciprete, C. Sibilia, M. Bertolotti, I. Nefedov, and I. V. Anoshkin, "Photoacoustic characterization of randomly oriented silver nanowire films," Int. J. Thermophys. **36**, 342–348 (2015).
163. G. Cesarini, G. Leahu, M.L. Grilli, A. Sytchkova, C. Sibilia, and R. Li Voti, "Optical and photoacoustic investigation of AZO/Ag/AZO transparent conductive coating for solar cells," Phys. Status Solidi C **13**(10-12), 998–1001 (2016).
164. E. Petronijevic, G. Leahu, V. Mussi, C. Sibilia, and F.A. Bovino, "Photoacoustic technique for the characterization of plasmonic properties of 2D periodic arrays of gold nanoholes," AIP Adv. **7**(2), 025210 (2017).
165. G. Leahu, E. Petronijevic, A. Belardini, M. Centini, R. Li Voti, T. Hakkarainen, E. Koivusalo, M. Guina, and C. Sibilia, "Photo-acoustic spectroscopy revealing resonant absorption of self-assembled GaAs-based nanowires," Sci. Rep. **7**(1), 2833 (2017).
166. S.J. Zelewski, J. Kopaczek, W.M. Linhart, F. Ishikawa, S. Shimomura, and R. Kudrawiec, "Photoacoustic spectroscopy of absorption edge for GaAsBi/GaAs nanowires grown on Si substrate," Appl. Phys. Lett. **109**(18), 182106 (2016).
167. E. Petronijevic, G. Leahu, A. Belardini, M. Centini, R. Li Voti, T. Hakkarainen, E. Koivusalo, M. Rizzo Piton, S. Suomalainen, M. Guina, and C. Sibilia, "photo-acoustic spectroscopy reveals extrinsic optical chirality in GaAs-based nanowires partially covered with gold," Int. J. Thermophys. **39**(3), 45 (2018).
168. R. Li Voti, G. Leahu, E. Petronijević, A. Belardini, T. Cesca, C. Scian, G. Mattei, and C. Sibilia, "Characterization of chirality in diffractive metasurfaces by photothermal deflection technique," Appl. Sci. **12**(3), 1109 (2022).
169. C. Kuppe, C. Williams, J. You, J.T. Collins, S.N. Gordeev, T.D. Wilkinson, N. Panoiu, and V.K. Valev, "Circular dichroism in higher-order diffraction beams from chiral quasiplanar nanostructures," Adv. Opt. Mater. **6**(11), 1800098 (2018).
170. C. Kuppe, X. Zheng, C. Williams, A.W.A. Murphy, J.T. Collins, S.N. Gordeev, G.A.E. Vandenbosch, and V.K. Valev, "Measuring optical activity in the far-field from a racemic nanomaterial: diffraction spectroscopy from plasmonic nanogratings," Nanoscale Horiz. **4**(5), 1056–1062 (2019).
171. M. Yamauchi, K. Mawatari, A. Hibara, M. Tokeshi, and T. Kitamori, "Circular dichroism thermal lens microscope for sensitive chiral analysis on microchip," Anal. Chem. **78**(8), 2646–2650 (2006).
172. V.K. Valev, J.J. Baumberg, C. Sibilia, and T. Verbiest, "Chirality and chiroptical effects in plasmonic nanostructures: fundamentals, recent progress, and outlook," Adv. Mater. **25**(18), 2517–2534 (2013).

Optical Materials EXPRESS

173. E.A. Mamonov, T.V. Murzina, I.A. Kolmychek, A.I. Maydykovsky, V.K. Valev, A.V. Silhanek, T. Verbiest, V.V. Moshchalkov, and O.A. Aktsipetrov, "Chirality in nonlinear-optical response of planar G-shaped nanostructures," Opt. Express **20**(8), 8518–8523 (2012).
174. V.K. Valev, A.V. Silhanek, N. Verellen, W. Gillijns, P. Van Dorpe, O.A. Aktsipetrov, G.A.E. Vandenbosch, V.V. Moshchalkov, and T. Verbiest, "Asymmetric optical second-harmonic generation from chiral G-shaped gold nanostructures," Phys. Rev. Lett. **104**(12), 127401 (2010).
175. V.K. Valev, N. Smisdom, A.V. Silhanek, B. De Clercq, W. Gillijns, M. Ameloot, V.V. Moshchalkov, and T. Verbiest, "Plasmonic ratchet wheels: switching circular dichroism by arranging chiral nanostructures," Nano Lett. **9**(11), 3945–3948 (2009).
176. D.C. Hooper, A.G. Mark, C. Kuppe, J.T. Collins, P. Fischer, and V.K. Valev, "Strong rotational anisotropies affect nonlinear chiral metamaterials," Adv. Mater. **29**(13), 1605110 (2017).
177. A. Belardini, G. Leahu, E. Petronijevic, T. Hakkarainen, E. Koivusalo, M. Rizzo Piton, S. Talmila, M. Guina, and Concita Sibilia, "Circular dichroism in the second harmonic field evidenced by asymmetric au coated GaAs nanowires," Micromachines **11**(2), 225 (2020).
178. D. L. Andrews and T. Thirunamachandran, "Hyper-Raman scattering by chiral molecules," J. Chem. Phys. **70**(2), 1027 (1979).
179. J. T. Collins, K. R. Rusimova, D. C. Hooper, H.-H. Jeong, L. Ohnoutek, F. Pradaux-Caggiano, T. Verbiest, D. R. Carbery, P. Fischer, and V. K. Valev, "First observation of optical activity in hyper-Rayleigh scattering," Phys. Rev. X **9**, 011024 (2019).
180. L. Ohnoutek, H. Jeong, R.R. Jones, J. Sachs, B.J. Olohan, D. Răsădean, G. Dan Pantoş, D.L. Andrews, P. Fischer, and V.K. Valev, "Optical activity in third-harmonic Rayleigh scattering: a new route for measuring chirality," Laser Photonics Rev. **15**(11), 2100235 (2021).
181. L. Ohnoutek, J. Kim, J. Lu, B.J. Olohan, D.M. Răsădean, G.D. Pantoș, and N.A. Kotov, and V.K. Valev, "Third-harmonic Mie scattering from semiconductor nanohelices," Nat. Photonics **16**(2), 126–133 (2022).
182. S. Hashiyada, T. Narushima, and H. Okamoto, "Local optical activity in achiral two-dimensional gold nanostructures," J. Phys. Chem. C **118**(38), 22229–22233 (2014).
183. S. Hashiyada, T. Narushima, and H. Okamoto, "Imaging chirality of optical fields near achiral metal nanostructures excited with linearly polarized light," ACS Photonics **5**(4), 1486–1492 (2018).
184. M. Schnell, P. Sarriugarte, T. Neuman, A.B. Khanikaev, G. Shvets, J. Aizpurua, and R. Hillenbrand, "Real-space mapping of the chiral near-field distributions in spiral antennas and planar metasurfaces," Nano Lett. **16**(1), 663–670 (2016).